CFD BASED DESIGN AND ANALYSIS OF BUILDING MOUNTED WIND TURBINE WITH DIFFUSER SHAPED SHROUD

ABILASH KRISHNAN

A Thesis
In the Department
Of
Mechanical and Industrial Engineering

Presented in Partial Fulfilment of the Requirements
For the Degree of
Master of Applied Science (Mechanical Engineering) at
Concordia University
Montréal, Québec, Canada

July 2015

Concordia University

School of

Graduate Studies

This is to certify that the thesis prepared

By: **Abilash Krishnan**

Entitled : CFD Based Design and Analysis of Building Mounted VAWT with Diffuser Shaped Shroud

and submitted in partial fulfilment of the requirements for the degree of

Master of Applied Science (Mechanical Engineering)

Complies with the regulations of the university and meets the acceptable standards with respect to originality and quality.

Signed by the final examining committee :

_______Christian Moreau__________ (Chair)
_______Ali Dolatabadi____________ (Examiner)
_______Samuel Li_______________(Examiner)
_______Marius Paraschivoiu_______ (Supervisor)

Approved by ____

MASc Program Director

Department of Mechanical and Industrial Engineering

____ /____ / 2015

____

Dean of Faculty

ABSTRACT

CFD Based Design and Analysis of Building Mounted VAWT with Diffuser Shaped Shroud

Abilash Krishnan

The production of sustainable energy is one of the biggest challenges facing us today. Wind and solar technologies are the leaders for clean energies. Wind energy is in relatively plentiful supply, can be used efficiently and is a nonpolluting power production method. Within this paradigm, building-integrated micro wind turbines are promising low cost renewable energy devices, but are fraught with challenges like low wind speeds and high turbulence intensity. In this thesis, a comprehensive study of increased performance of a wind turbine design inside a diffuser shaped shroud on building roofs is conducted. A commercial Computational Fluid Dynamics (CFD) model is used to simulate unsteady 3D flows inside the diffuser and around the turbine. The meshing strategy and model used is verified using a grid refinement study. The geometric modifications and various non-dimensional parametric studies conducted are also described in detail, along with the relevant discussion of results obtained. Furthermore, the coefficient of power of the turbine is improved from 0.135 to 0.394, representing an improvement of almost 300%. This improvement can largely be attributed to the flanged diffuser shroud design, as well as the modifications made to the blades of the turbine.

ACKNOWLEDGEMENTS

I would like to thank my thesis advisor, Dr. Marius Paraschivoiu, for his constant support and encouragement. His calm yet challenging demeanor and approachable personality has helped me overcome many obstacles over the course of my research, and strive to produce the best possible work. I would also like to thank Le Groupe LML for their co-operation and help in completing this work successfully.

I thank Matin Komeili, Patrick Larin and Gabriel Naccache for their helpful suggestions along the way. I also extend my gratitude to the ENCS department at Concordia University, for providing me with the necessary facilities to complete my research.

A special mention goes to my dear friends Kenneth Macintosh, Stephanie Gallant, Danielle Nash, Adrian Dimech, Hugo O'Doherty and Krishna BV, for always standing by me, supporting me and unconditionally loving me.

Finally, I am eternally grateful to my loving parents AEA Krishnan and Radhika Krishnan, and my sister, Anisha Krishnan, who have constantly guided and nurtured me to the best of their abilities. They are and will continue to be my strongest pillars of strength and unwavering support. I would like to dedicate my thesis to them.

CONTENTS

LIST OF FIGURES

LIST OF TABLES

NOMENCLATURE

SYMBOL	PROPERTY
$\vec{u}$	Velocity vector
P	Pressure
$\vec{F}$	Force vector
ρ	Density of air
μ	Dynamic viscosity of air
$\overline{P}$	Mean pressure
P'	Fluctuating component of pressure term
$\overline{u_\iota}$	Mean velocity
$u_i{}'$	Fluctuating component of velocity
R_{ij}	Reynold's stress tensor
$\mu_t.$	Eddy viscosity / effective turbulent viscosity
k	Turbulent kinetic energy
ϵ	Turbulent dissipation rate
λ	Tip speed ratio
V_∞	Free stream velocity
ω	Angular speed of turbine rotor
R	Blade tip radius of rotor
C_p	Coefficient of power
A	Swept area of turbine
H'	Height of building

ν	Kinematic viscosity of air
h	Characteristic length in a grid
N	Number of elements in grid
r	Refinement ratio between two grids
θ_{diff}	Angle between ceiling of downwind portion of flanged diffuser to the horizontal
Y	Length of ramp of turbine
θ_{cut}	Angle of blade that is cut
N_{blades}	Number of blades in a configuration

CHAPTER 1 : INTRODUCTION

1.1. IMPORTANCE OF RENEWABLE ENERGY

Energy is an extremely vital human need today, being essential to all modern day activities including household, transportation, industry, agriculture, education and communication. Availability of energy in societies also directly influences their economic wellbeing. A lot of problems, environmental and non-environmental, are caused by the fact that the majority of this energy comes from fossil fuels such as coal, oil and natural gas. Some of the major environmental consequences of using fossil fuels include high carbon dioxide (CO_2) emissions that pollute the atmosphere; depletion of forested areas, which has worsened global warming; and, very importantly, these energy resources are non-renewable and will eventually run out [1]. We need not look too far back in history to find examples that show us the devastating implications of indiscriminate consumption of fossil fuels. 11 human lives were lost along with a massive oil spill in the Gulf of Mexico in April 2010 when an oil rig exploded [2]. Apart from the associated environmental issues, the use of fossil fuels also has other problems, which include price fluctuations and concerns about security of supply.

Various solutions are being researched as it becomes apparent that we cannot rely solely on conventional energy resources like coal, natural gas and petroleum. Among these possible solutions, renewable energy (solar power, wind power, hydropower, biomass, geothermal power, and wave and tidal power) is widely regarded as drastically important for a sustainable energy future [3]. By using renewable energy, we have the power to eliminate or at least minimize the safety issues related to the use of fossil fuels and atomic energy [4]. Moreover, renewable energy reduces greenhouse gas emissions, increasing environmental quality and helping us in the fight against climate change. There are also no process costs and equipment required to collect renewable energy resources since they are sustainable, free and practically omnipresent.

The global awareness of the need for RE has increased considerably in recent years as more and more countries are shifting their energy generation to RE resources [5]. RE projects are making significant contributions to the national energy supplies of many countries across the world while helping to preserve the environment [6], [7], [8], [9], [10]. According to The Energy Report 2011, World Wide Fund for Nature (WWF), the RE supply will be sufficient to fulfil the global energy needs by 2050 and will save almost £4 trillion per year through energy efficiency and reduced fuel costs [11]. RE supplied an estimated 19% of the global final energy consumption by the end of 2012; with approximately 9% coming from traditional biomass and 10% from modern renewables sources.

However renewable energy also has its drawbacks. One cannot overstate the importance of identifying the right type of renewable technology for a particular country or region. Factors that must be optimized include costs related to the generation of electricity, the efficiency of the chosen system, the land and water requirements and also the social and economic impact related to their implementation have to be taken into account [12]. In the following section, we will look more closely at one specific renewable resource relevant to this thesis : Wind Energy.

1.2. IMPORTANCE OF WIND ENERGY

Wind energy is a major resource of electricity generation among other renewable resources, after hydropower [13]. Wind turbines provided 1.5% of the worldwide electricity usage in 2008 [14]. Further, in the next two decades, a lot of very promising development is expected in the field of wind energy [15]. It is envisioned that the global cumulative wind power capacity will be increased up to 832,251 MW and 1,777,550 MW in the years 2020 and 2030, respectively. It is worth noting that the computed capacity in 2009 was approximately 158,505 MW. By means of this quantitative comparison, it can be conclude that the wind power provides approximately one-sixth of the world's electricity. This accounts for land and offshore-wind farms as well as industrial wind turbines.

While there are disadvantages also associated with wind energy, they are far overshadowed by the disadvantages of other renewable sources of energy [16].

Solar energy has a very high initial cost due to the cost of purchasing and installing solar panels. Further the location of solar panels has to be in areas that are not cloudy or foggy. The photovoltaic panels are made of silicon and other toxic metals like mercury, lead and cadmium. Their efficiency is also susceptible to pollution. They are also quite inefficient, useless at night and require large installation areas.

Hydropower suffers from various disadvantages as well such as large emissions of methane and carbon dioxide. The formation of large and huge dams destroys the living beings around them, local life is disturbed, and plants are destroyed. While the effective cost is zero, manufacturing and building a dam, maintenance and installation of turbines is very costly. It is only useful in areas with a good amount of rainfall. Further dams alter the natural system of water, affect the amount, quality and temperature of water that flow in streams, and the water, while flowing through the dam, collects nitrogen which can damage and even kill fish.

Nuclear power is also not free of a number of disadvantages. The waste produced by nuclear reactors is extremely hazardous and can leak radiations. Nuclear accidents like the one in Chernobyl pose a significant potential threat. Setting up a nuclear power station is extremely expensive and take between five to ten years to construct. The reactors also have a significant impact on aquatic and human life. Uranium is a very scarce resource and only exists in few countries, hence this source of energy is technically not even renewable.

Geothermal energy, unfortunately, is not a widespread source of energy. It has very high installation costs, and geothermal sites can run out of steam over a period of time due to drop in temperature or if too much water is injected to cool the rocks. It is only suitable for regions which have hot rocks below the Earth. The sites may contain poisonous gases. Further, it is very difficult to transport geothermal energy. Once the tapped energy is extracted, it can only be used in the surrounding areas.

Thus it is quite clear that among the renewable sources of energy, wind energy is worth researching and propagating because of how clean it is, and its feasibility.

1.3. TYPES OF WIND TURBINES

Wind turbines are classified based on their axis of rotation. Basically, there are two types of wind turbines, namely Horizontal Axis Wind Turbines (HAWTs) and Veritcal Axis

Wind Turbines (VAWTs). The majority of currently installed wind turbines belongs to HAWTs. However, some important advantages of VAWTs make them to be widely applicable in urban areas. A VAWT is a type of wind turbine which has the main rotor located vertically and the gear box is placed near the ground. Therefore, in comparison with HAWTs, maintenance and repair level compliance requirements are facilitated. In addition to the maintenance facility, VAWTs provide significant advantages which make them to be a better choice. Most importantly, VAWTs can be placed close to each other. As a result, less space is occupied compared to HAWTs. Furthermore, less noise is produced and also the starting speed to move the blades is much less than HAWTs. Generally, HAWTs provide better performance in the uniform wind but their performance becomes less as the wind direction fluctuates [17]. Hence, for any direction, non-uniformity or even the rapid fluctuations of the wind, VAWTs operate better [18] and also, dirty winds have less effects on their performance. Besides, VAWT blades have a uniform and untwisted profile which makes their fabrication easier compared to HAWTs which blade should be tapered and twisted in order to gain the optimal efficiency. The major drawbacks are the lack of self-starting capability as well as its high torque fluctuations within each revolution cycle [19] [20]. Moreover, due to rotational motion of the wind turbines, dynamics stall and fatigue failure may occur.

1.4. MOTIVATION

Building-integrated micro-wind turbines are promising low-cost renewable energy devices. However, the take-up of micro-wind turbines in high density suburban environments is still very limited due to issues such as: a) low wind speeds; b) high turbulence intensity; and c) the perception of potentially high levels of aerodynamic noise generated by the turbines. The wind flow field above the roof of buildings in this environment is different to that over flat terrain or around isolated buildings. Thus optimal location of roof mounted wind turbines is of paramount importance [21].

Further, wind power generation is proportional to the wind speed cubed. If we can increase the wind speed with some mechanism by utilizing the fluid dynamic nature around a structure or topography, namely if we can capture and concentrate the wind energy locally, the output power of a wind turbine can be increased substantially. This facilitates us to utilize power in a more efficient way. One such method is the flanged diffuser concept, which is discussed in this thesis. It is also applied to the turbine being studied, and is seen to aid significantly in the generation of power. The flange causes the creation of vortices behind itself, which gives rise to a low pressure region. This low pressure region is responsible for drawing in more flow and thus increasing the net mass flow into the turbine.

Hence the motivation behind the research conducted is to find a viable way to generate electricity at the site of usage, and utilize the advantages of location associated with the roof of the building, while minimizing the disadvantages of flow interaction with the building. It is also extremely vital to shepherd the design process towards a turbine that can consistently produce electricity at low wind speeds, with good efficiency, as this is relevant to the paradigm of urban rooftop wind turbines.

1.5. OBJECTIVES

1.5.1. To use the CFD tool efficiently

It is necessary to properly understand the various parameters relevant to the analyses that will be conducted. This includes meshing strategy, boundary conditions, type of solver etc. Each of the parameters must be accurate and pertinent to the study being conducted. This must also be validated.

1.5.2. To implement the flanged diffuser concept and increase the mass flow into the turbine

The mass flux into the turbine can be significantly increased through proper understanding of the geometry of the shroud encasing the turbine. Using this, the power coefficient of the turbine can be improved greatly.

1.5.3. To conduct a parametric study of the most pertinent factors of design such as blade length, number of blades, position of turbine etc.

It is interesting to properly understand the effect each factor of design has on the efficiency of the turbine. Using this, a final design can be arrived at that optimizes all of these factors.

1.5.4. To present a final design of the turbine along with the shroud, by choosing the optimum values from the above mentioned parametric studies.

1.6. LITERATURE REVIEW

A number of studies have been conducted on the feasibility of wind power generation and the role it can play in helping us attain a sustainable future. In one such study, Soder et al [22] have studied regions where wind power produces up to 35% of yearly gross demand. They discovered that in all these areas, the maximal wind power is considerably less than minimum load plus export possibility. Thus, while the current penetration of wind power is small, especially in countries with excellent wind resources (like Ireland), there is a lot more scope for generation of wind power.

In many of the wind turbine simulations, CFD analysis has been used to predict performance to a remarkable degree of accuracy. However, it is extremely important to set up this CFD analysis in the correct way. Sanderse et al [23] have reviewed the latest numerical calculations of wind turbine wake aerodynamics, and discussed the CFD techniques for modelling the rotor and the wake of the turbine, especially with emphasis on the wake effect on downstream turbines. Song et al. [24] have studied four meshing strategies and six different turbulence model selections for VAWT simulations. While this study was only 2D, it was established that the realizable $k-\epsilon$ model enables the closest CFD simulation of the experimental model and also shows the best prediction performance. It is worth noting here that they also stipulate that the rotation angle in each time step should not exceed two degrees. Sagol et al [25] have studied prediction using the two-equation turbulence models in ANSYS FLUENT for a NREL Phase VI HAWT rotor, for a particular wind speed. They found that the $k-\omega$ SST model is the most appropriate. This model is generally considered to be the industrial standard, but requires certain stringent mesh requirements, and involves a higher computational cost and time.

Significant research has been conducted on the flow of air or wind around buildings. Holdredge et al [26] and Evans [27] have studied the air flow over a building, and found that a positive pressure zone is created on the upstream side, while negative pressure zones (recirculation zones) are created on the roof and all other sides. For air flow perpendicular to the wind-ward wall, the height of the roof recirculation zone may be approximately 1.3 to 2 times the building height of conventional one and two storey industrial buildings. While the cavity will extend over the entire roof the building for many buildings, if the building is very long in the wind direction, then the air flow will re-attach to the roof. Further, Song et al [28] studied the large-scale vortex structure and the unsteady behavior of flow around a tall building. They discovered that a horse-shoe vortex develops around the building. Twin axial vortices are produced by the roof side edges, like tip vortices, which are then strengthened by the downwash from the main stream. There is also unsteady vortex shedding on the vertical plane of symmetry, induced by Karman vortex shedding.

Azli Abd Razak et al [29] have conducted Large Eddy Simulation (LES) around five different types of uniform staggered building arrays, to simulate the pedestrian wind environment. They found that the frontal area ratio, which is the product of the plan area ratio and building aspect ratio, is the most important parameter in estimating the pedestrian wind environment. A simple exponential equation was derived to predict the pedestrian wind environment as a function of the frontal area ratio. Islam Abohela et al [30] established that a significant increase (up to 56.1%) in energy output can be achieved on roof mounted wind turbines, with a vaulted roof, and an informed wind assessment. However, the turbine used for this analysis was not shrouded in any manner. Abohela et al [31] also found that changing wind direction, building height and surrounding urban configuration had an effect on choosing the optimum mounting location of the turbine and its energy yield. A feasible solution would be to inform developers of buildings on which roof shape to be used and how to orient the building in a way in which the roof mounted wind turbine could benefit from the prevailing wind direction and its interaction with the proposed roof shape. While a compromise would have to be arrived at, regarding the orientation of the building, the roof shape and other architectural requirements, such integration could results in new types of buildings.

Research has also been conducted on the possibility of accelerating the wind flow into the turbine, thus increasing the power available. Ohya et al [32] have shown that a wind turbine system that consists of a diffuser shroud with broad-ring brim at the exit periphery and a wind turbine inside it, demonstrates power augmentation for a given turbine diameter and wind speed by a factor of about 2-5 compared with a bare wind turbine. This is because a low-pressure region due to a strong vortex formation behind the broad brim draws more mass flow to the wind turbine inside the diffuser shroud.

The novelty of this study lies in the fact that besides being a parametric study of the rooftop mounted wind turbine, every simulation is conducted with both the turbine and the building. Thus all the effects of the building upon the air flow are accounted for, and indeed, in certain cases are also used to the benefit of the turbine design.

1.7. THESIS OUTLINE

This section briefly discusses the organization of this thesis, with some salient points of each chapter.

Chapter 2 outlines the methodology for the turbine design and analysis process. The governing equations relevant to the physics being studied are presented, followed by the different turbulence models available and the one that has been selected. Some non-dimensional parameters that are key to the design process are explained. Further the meshing strategy is clearly outlined along with the relevant parameters that have been selected. The wall treatment is discussed and the computational domain is presented. Finally the numerical setup is described in detail, with emphasis on the boundary conditions employed, the solver chosen and solution parameters.

Chapter 3 describes the verification process utilized to validate the model that is used. Three progressively refined meshes are analyzed and presented, and it is shown that the mesh used for the purpose of design analysis is sufficiently accurate.

Chapter 4 sequentially presents the 3D results obtained for each of the parts of the turbine being studied i.e. the shroud, the turbine blade and the position of the turbine respectively. Non dimensional parametric studies are discussed with respect to each of these parts. A reference study is conducted on a Banki turbine inside the shroud, to provide a point of comparison for the turbine being analyzed.

Chapter 5 discusses the final design obtained after having additively integrated all the optimized results presented in Chapter 5. A study is performed to find the optimal tip speed ratio (TSR) of this final design of the turbine. Finally overall conclusions are presented, along with objectives achieved, and scope of future work.

CHAPTER 2 : METHODOLOGY

This chapter presents the methodology used to conduct the simulations relevant to this thesis. Each parameter is explored, including governing equations, meshing strategy, solution parameters and choice of solver. It is also discussed in detail which option is chosen, and how this option fits into the paradigm for this analysis.

2.1. GOVERNING EQUATIONS

Aerodynamic analysis is one of the most critical steps in designing wind turbines. The three formulations that are generally used to perform such analyses are as follows:

(i) Integral formulations/BEM methods [33], in which the rotor blade is modeled by the actuator disc concept and blade element theory, and the flowfield is described by the integral momentum equation.

(ii) Hybrid methods [34], in which the flowfield is described either by Navier-Stokes or Euler equations and the rotor blade is modeled by a generalized actuator disc concept.

(iii) Full Navier-Stokes methods [35] in which the flowfield is described by Navier-Stokes equations and the rotor blade is introduced by it real geometrical shape using moving reference frame or moving mesh technique.

The BEM methods have demonstrated their capabilities for performance predictions, as well as conception and design of wind turbines within a limited range of wind-speeds (normal flow conditions). There are a number of situations where it is not reasonable to expect BEM methods to offer the desired accuracy, however. In fact, despite the advantage of low computations requirements, these methods cannot describe accurately three dimensional unsteady effects (e.g., turbulence, separated flow etc.) and rarely provides detailed aerodynamic information.

The complex flow conditions that rotor encounter can be described adequately by the formulations pertaining to the two last classes. Between these two, the full Navier-Stokes methods are expected to perform more accurate aerodynamic predictions by using modern computational fluid dynamics (CFD) tools. This is the formulation that is chosen for the purpose of this study.

The flow over the wind turbine falls within the regime of incompressible and transient. Thus simulation of the flow over the VAWT is studied by seeking the numerical solution of RANS equations coupled with a turbulence model.

The incompressible Navier-Stokes equations for Newtonian fluids are,

$$\nabla.\vec{u} = 0 \tag{2.1}$$

$$\frac{\partial \vec{u}}{\partial t} + (\vec{u}.\nabla)\vec{u} = -\frac{1}{\rho}\nabla P + \frac{\mu}{\rho}\nabla^2\vec{u} + \vec{F} \tag{2.2}$$

These can also be written as

$$\frac{\partial u_i}{\partial x_i} = 0 \tag{2.3}$$

$$\frac{\partial u_i}{\partial t} + \frac{\partial}{\partial x_j}\left(u_i u_j\right) = -\frac{1}{\rho}\frac{\partial P}{\partial x_i} + \frac{\mu}{\rho}\frac{\partial^2 u_i}{\partial x_j} \tag{2.4}$$

Where $i, j \in \{1,2,3\}$

2.2. TURBULENCE MODEL

There are three main approaches to turbulence modelling that can be used.

1. **Reynolds' Averaged Navier Stokes (RANS) models** : In this set of models, the Navier Stokes equations are solved for time-averaged flow behavior and magnitude of turbulent fluctuations.
2. **Eddy Simulation Models** : These models are more advanced than the RANS models for resolving turbulence. However they require much better mesh resolution and have very long computational run times.
3. **Direct Numerical Simulation (DNS)** : Here every fluctuating motion in the flow is resolved. A very fine grid is required with a very small time step. Further the demands of the mesh and time step increase as the Reynolds' number increases.

For our purpose, the RANS models are sufficient and deliver good results, while not being excessively computationally expensive. Hence this approach has been chosen.

In order to derive RANS equations, Reynolds decomposition is carried out. Each instantaneous flow variable, is expressed as the sum of the mean and the fluctuating components.

$$P = \overline{P} + P' \tag{2.5}$$

$$u_i = \overline{u_i} + u_i' \tag{2.6}$$

Furthermore, time averaging is defined as

$$\overline{u_i} = \lim_{T\to\infty} \frac{1}{T}\int_0^T u(x_i, t)dt \tag{2.7}$$

Applying Reynolds decomposition and taking time-average of the continuity and momentum equations yields the following RANS equations as follows,

$$\frac{\partial \overline{u_i}}{\partial x_i} = 0 \tag{2.8}$$

$$\frac{\partial \overline{u_i}}{\partial t} + \frac{\partial}{\partial x_j}\left(\overline{u_i}\,\overline{u_j}\right) = -\frac{1}{\rho}\frac{\partial \bar{P}}{\partial x_i} + \frac{\mu}{\rho}\frac{\partial^2 \overline{u_i}}{\partial x_j} + \frac{\partial R_{ij}}{\partial x_j} \tag{2.9}$$

Here

$$R_{ij} = -\overline{u_i' u_j'} \tag{2.10}$$

The Reynolds' stress tensor R_{ij} is an additional symmetric tensor which has six independent components and expresses the correlation between the fluctuating velocities.

Now, RANS models fall into one of two categories. The difference in these is how R_{ij} is calculated.

In the Eddy Viscosity Models (EVM), an isotropy assumption is made, i.e. it is assumed that stress is directly proportional to strain (strain being the gradients of velocity). This assumption is called the Boussinesq assumption. A new unknown quantity needed by EVMs is the effective turbulent viscosity or eddy viscosity, μ_t.

$$-\rho\overline{u_i' u_j{}'} = \mu_t\left(\frac{\partial \overline{u_i}}{\partial x_j} + \frac{\partial \overline{u_j}}{\partial x_i}\right) - \frac{2}{3}\delta_{ij}\left(\rho k + \mu_t\frac{\partial \overline{u_m}}{\partial x_m}\right) \tag{2.11}$$

The eddy viscosity is very relevant, as it will be used later to check the accuracy of the boundary layer resolution.

In the Reynolds' Stress Models (RSM), a transport equation is derived for the Reynolds' stress terms. This model might be more accurate for certain cases, as the stresses are considered anisotropic. However, this model is more complex, since there are more equations to solve. There are also further unknowns, which themselves require a model.

It is not practical to use the Reynolds' Stress Model as it is extremely computationally expensive. However in our particular simulation, the Boussinesq assumption is invalid. The realizable $k-\epsilon$ model is an Eddy Viscosity Model, belonging to the family of $k-\epsilon$ turbulence models. It has been developed to address the shortcoming of the Boussinesq assumption [36].

The transport equations for k and ϵ in the realizable $k-\epsilon$ model are given as

$$\frac{\partial(\rho k)}{\partial t}+\frac{\partial}{\partial x_j}\left(\rho k u_j\right)=\frac{\partial}{\partial x_j}\left[\left(\mu+\frac{\mu_t}{\sigma_k}\right)\frac{\partial k}{\partial x_j}\right]+G_k+G_b-\rho\epsilon-Y_M+S_k \tag{2.12}$$

And

$$\frac{\partial(\rho\epsilon)}{\partial t}+\frac{\partial}{\partial x_j}\left(\rho\epsilon u_j\right)=\frac{\partial}{\partial x_j}\left[\left(\mu+\frac{\mu_t}{\sigma_\epsilon}\right)\frac{\partial\epsilon}{\partial x_j}\right]+\rho C_1 S\epsilon-\rho C_2\frac{\epsilon^2}{k+\sqrt{v\epsilon}}+C_{1\epsilon}\frac{\epsilon}{k}C_3 G_b+S_\epsilon \tag{2.13}$$

Where

$$C_1=\max\left[0.43,\frac{\eta}{\eta+5}\right] \tag{2.14}$$

$$\eta=S\frac{k}{\epsilon} \tag{2.15}$$

$$S=\sqrt{2S_{ij}S_{ij}} \tag{2.16}$$

$$\mu_t=\rho C_\mu\frac{k^2}{\epsilon} \tag{2.17}$$

The major difference between the realizable $k - \epsilon$ model and the standard $k - \epsilon$ model is that in the former, the determination of C_μ is not a constant. It is instead calculated as follows.

$$C_\mu = \frac{1}{A_0 + A_S \frac{kU^*}{\epsilon}} \tag{2.18}$$

Where

$$U^* = \sqrt{S_{ij}S_{ij} + \widetilde{\Omega_{ij}}\widetilde{\Omega_{ij}}} \tag{2.19}$$

And

$$\widetilde{\Omega_{ij}} = \Omega_{ij} - 2\epsilon_{ijk}\omega_k \tag{2.20}$$

$$\Omega_{ij} = \overline{\Omega}_{ij} - \epsilon_{ijk}\omega_k \tag{2.21}$$

The advantages of the realizable $k - \epsilon$ model is improved performance in flows with recirculation, strong pressure gradients, flow separation and the non-reliance on an assumed relationship between the Reynolds’ stress tensor and the strain rate tensor. Thus it is often used for the simulation of rotating zones. This is the model that has been chosen for the purpose of this study.

2.3. NON DIMENSIONAL PARAMETERS

2.3.1. Tip Speed Ratio λ

One important parameter in wind turbine investigations is Tip Speed Ratio, which is defined as the ratio of tip speed of the blade to the wind speed.

$$\lambda = \frac{R\omega}{V_\infty} \tag{2.22}$$

Here λ refers to the tip speed ratio, R refers to the tip radius, ω refers to the angular speed, and V_∞ refers to the free stream wind speed. This ratio gives an indication of how fast the turbine is rotating, with respect to the free stream velocity of air. It is extremely useful in optimizing the turbine's operating conditions for optimal performance.

2.3.2. Power Coefficient C_p

The Power Coefficient is another important parameter. It can be derived by applying the Pi-Buckingham theorem and is given by

$$C_p = \frac{P}{\frac{1}{2}\rho A V_\infty^3} \tag{2.23}$$

Here P refers to the power generated by the turbine, ρ refers to the density of air, A refers to the swept area of the turbine, and V_∞ refers to the free stream wind speed. This coefficient measures how efficient the turbine is, i.e. how much of the energy available in the wind it is able to access.

2.4. MESH SETUP :

Pre-processing is the phase before an analysis is run. This phase involves building the relevant geometry and generating a mesh which will be consequently converted into a format that can be read by the solver. This step is extremely important as in the majority of solvers, the accuracy of the numerical results obtained strongly depends on the quality of the mesh generated.

2.4.1. MULTIZONE MESHING

Meshes in CFD investigations can be classified as structured or unstructured. Structured types of grids are sets of elements which are repeated in a regular pattern with respect to space and are demonstrated by quadrilateral elements in 2D and hexahedral elements in 3D. Due to this regular arrangement, each cell can be directly addressed by means of an index (i, j) and (i, j, k) in 2D and 3D respectively, which helps save lots of computational efforts during the computation [37]. The natural ordering of elements in structured meshes also enables the construction of very efficient numerical algorithms to solve the flow equations. Grids of this type are especially applicable to the finite difference method because the variable differentiations and discretization can be expressed conveniently. While amenable to algorithmic efficiency, structured mesh are inherently difficult for discretizing complex geometries, as physical domains have to be decomposed into different subdomains (blocks) and the mesh has to be generated separately for individual blocks. Thus, in order to discretize complex geometries, unstructured meshes are used, where elements can be arbitrarily shaped (including triangular elements in 2D and tetrahedral elements in 3D). In addition to greater flexibility of geometry, these meshes also enable straightforward implementation of adaptive techniques where nodes may be added or deleted while mesh connectivity is updated locally, in order to enhance solution accuracy. Although unstructured meshes provide flexibility for discretizing complex geometries, they have the drawback of storing the connectivity information explicitly. Thus they require larger in-core memory and additional computational cost than their structured counterparts. Unstructured meshes are more widely used for finite element and finite volume approaches. It is worth mentioning here since the solver for this study (the commercial code FLUENT) utilizes the finite volume method, unstructured meshes are used for this simulation.

The choice of the type of mesh element to be employed depends on the delivered accuracy, efficiency and flexibility of the numerical solver. A two dimensional study [38] observed little difference in accuracy between equivalent meshes of quadrilateral and triangular elements. Hexahedral meshes have better accuracy than the tetrahedral meshes in three dimensional experiments [39]. In addition to reduced numerical error, hexahedral meshes also produced reduced element count, which is very useful as it leads to reduced computational cost. Furthermore, the element quality (a metric which enables us to identify how well a mesh will perform for a particular simulation) of hexahedral elements is often better than tetrahedral elements. One characteristic of quadrilateral/hexahedral elements that might make them more economical in some situations is that they permit a much larger aspect ratio than triangular/tetrahedral cells. A large aspect ratio in a triangular/tetrahedral cell will invariably affect the skewness of the cell, which is undesirable as it may impede accuracy and convergence. This is very beneficial for relatively simple geometries. They are also more consistent for convergence studies. Thus it is clear that wherever possible, hexahedral elements are the preferable option.

However, local refinement of a mesh is slightly more difficult with hexahedral elements. Further, tetrahedral elements lend themselves to be better adapted for more complex geometries. They also have the advantage that they can reduce element count in areas of non-interest in the domain, as the elements can be made quite large.
To leverage the advantages of both kinds of elements, a multi-zone method of meshing has been used for this simulation. In the area of interest, i.e. the moving mesh area around the turbine blades, hexahedral elements have been used. In the domain surrounding the

turbine casing and building, and the areas of the domain farther away from the building, tetrahedral elements have been used.

It is worth mentioning that for the geometry generation, the commercial ANSYS Design Modeler is used, while for the mesh generation, ANSYS Meshing is used [40].

2.4.2. WALL TREATMENT

The method of wall treatment depends largely on the nature of flow expected for a particular simulation. If boundary layer separation due to changing pressure gradient (and not sharp changes in geometry) is expected, then it is worthwhile to endeavor to resolve the boundary layer. However, for flows where wall-bounded effects are not a priority, or if separation is expected to occur only due to sharp changes in the geometry, an $\epsilon - based$ wall function approach is sufficient. Further, resolution of boundary layer requires a very fine mesh close to the walls, to ensure that sufficient nodes are located within the boundary layer region itself. This leads to extensive computational cost and thus, should only be used when absolutely necessary.

In the simulations relevant to this thesis, the wall bounded effects can be largely ignored. Thus the Standard Wall Function approach is used. This function assumes that the boundary layer mesh lies entirely within the log-law region, or the region where the average velocity of a turbulent flow at a certain point is proportional to the logarithm of the distance from that point to the wall.

y^+ is a parameter that indicates the non-dimensional distance. It is used to describe how coarse or fine a mesh is (especially near the wall). It is calculated as follows

$$y^+ = \frac{(yu_\tau)}{\nu} \tag{2.24}$$

where

$$u_\tau = \sqrt{\frac{\tau_w}{\rho}} \tag{2.25}$$

For the boundary layer mesh elements to be in the buffer region (where the log-law is applicable) it is essential that

$$y^+ > 30 \tag{2.26}$$

This is a constraint that has been enforced through all the meshes used in this thesis, to ensure the validity of the Standard Wall Function.

2.5. COMPUTATIONAL DOMAIN

The 3D computational domain for the simulation consists of two main zones : the cuboidal stationary zone which represents the far field flow and contains the building and turbine shroud, and the cylindrical moving zone which contains the seven turbine blades. The moving zone rotates with the designated angular velocity (which depends on the Tip Speed Ratio, or TSR). An interface is defined between the stationary and moving mesh zones. Figure 2.1 shows a schematic of the domain. Figures 2.2 through 2.5 present the mesh utilized for the simulation.

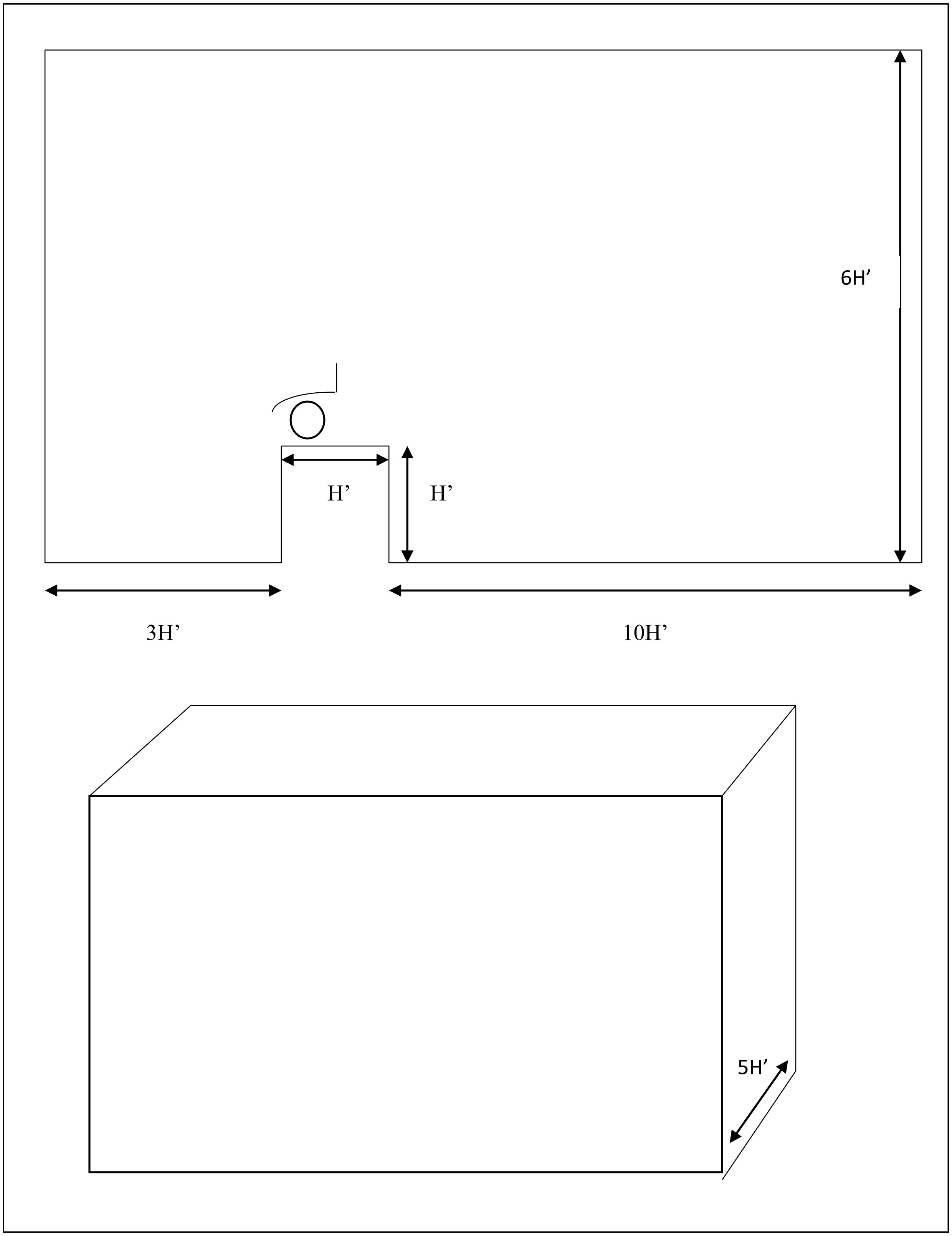

Figure 2.1: Schematic showing computational domain for simulation

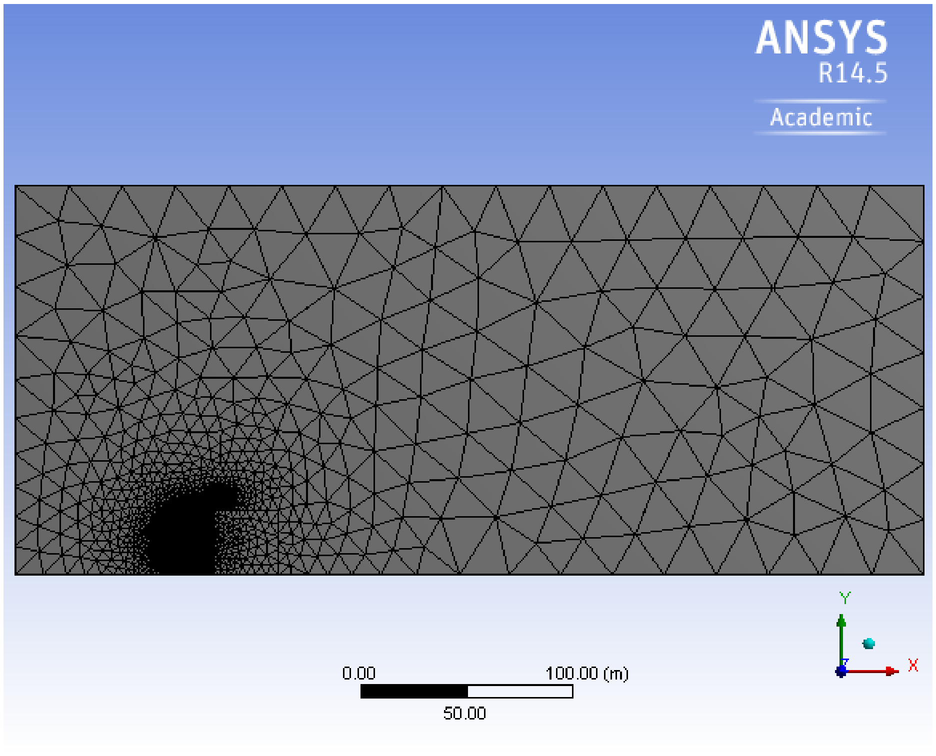

Figure 2.2: Side view of entire domain

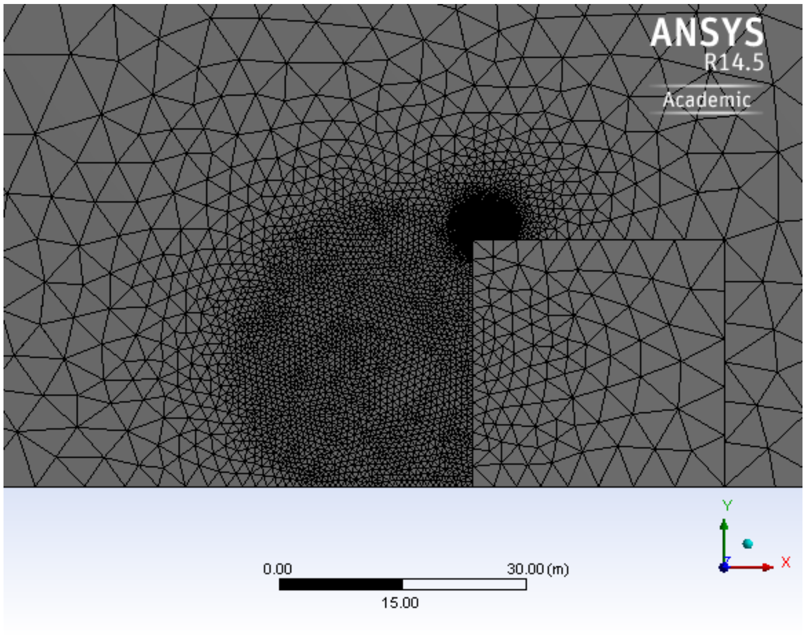

Figure 2.3: Side close-up view of turbine on building

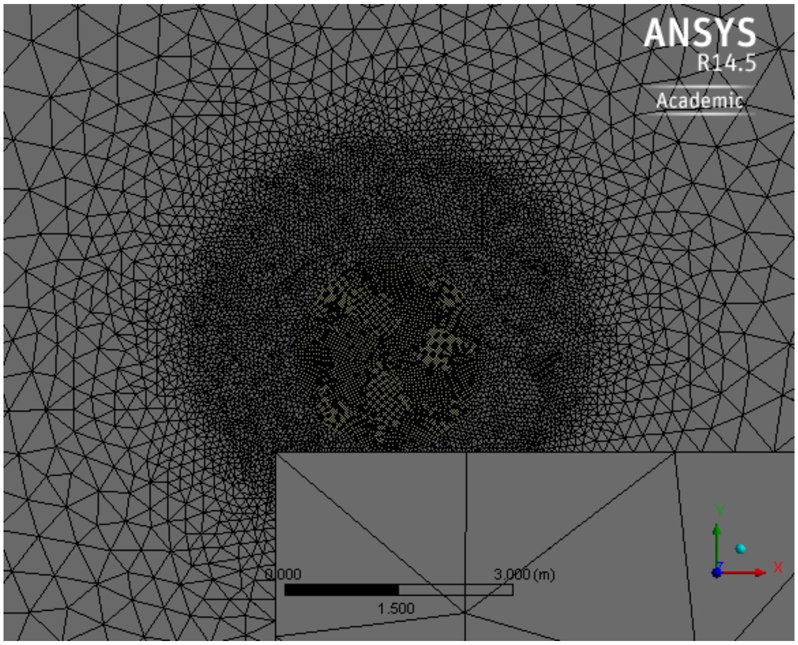

Figure 2.4: Side close-up view of turbine

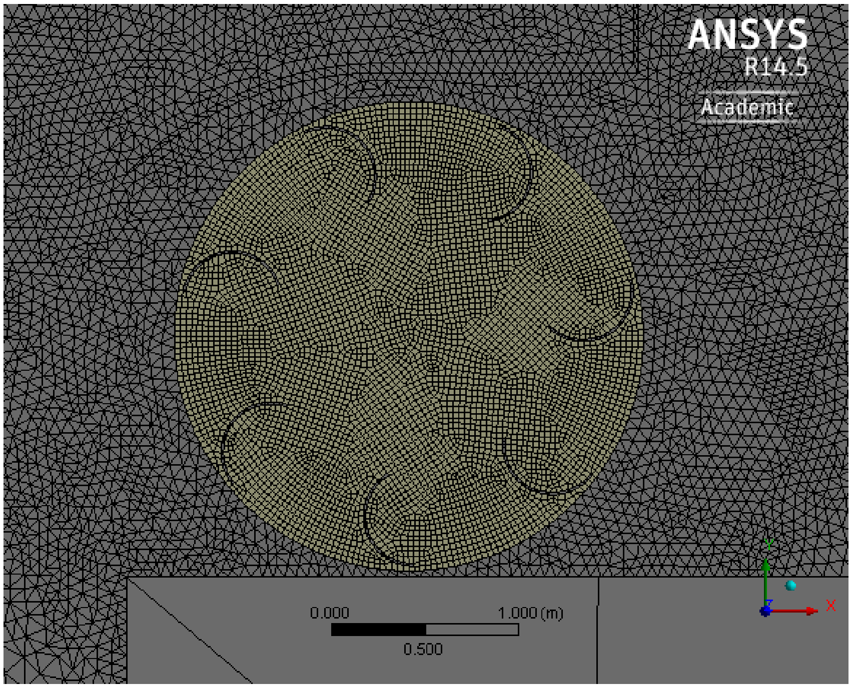

Figure 2.5: Side close-up view of turbine rotor

As indicated, H represents the height of the building used in the simulation ($H = 30.5m$). The distances between the building and the boundaries of the domain are indicated in the Figure 2.1 and have been maintained at these values to properly capture all the relevant physics associated with the simulation, without any interference due to the boundary conditions.

2.6. NUMERICAL SETUP:

The commercial software FLUENT has been used to carry out the CFD analysis. An incompressible transient state solver is used, with the moving mesh approach. In this approach, the mesh surrounding the rotor also rotates at each time step.

2.6.1. BOUNDARY CONDITIONS

In order to conduct a proper CFD simulation, it is essential to specify the initial and boundary conditions. Figure 2.6 presents a schematic showing the boundary conditions relevant to this simulation.

Note that only half the original domain is used for simulation as the symmetry boundary condition is applied on the face bisecting the turbine. An atmospheric boundary layer profile is used for the inlet condition at the upstream boundary as well as the boundary at the rear face of the cuboidal domain. This boundary layer profile is given by the equation:

$$v_h = v_H \left(\frac{h}{H}\right)^{0.31} \tag{2.27}$$

At the boundary on top of the domain, a constant tangential velocity is maintained. This velocity is same as the highest velocity on the upstream boundary. Atmospheric pressure is applied at the outlet condition at the downstream boundary. No slip boundary condition is assumed on the blades as well as the walls of the shroud and building.

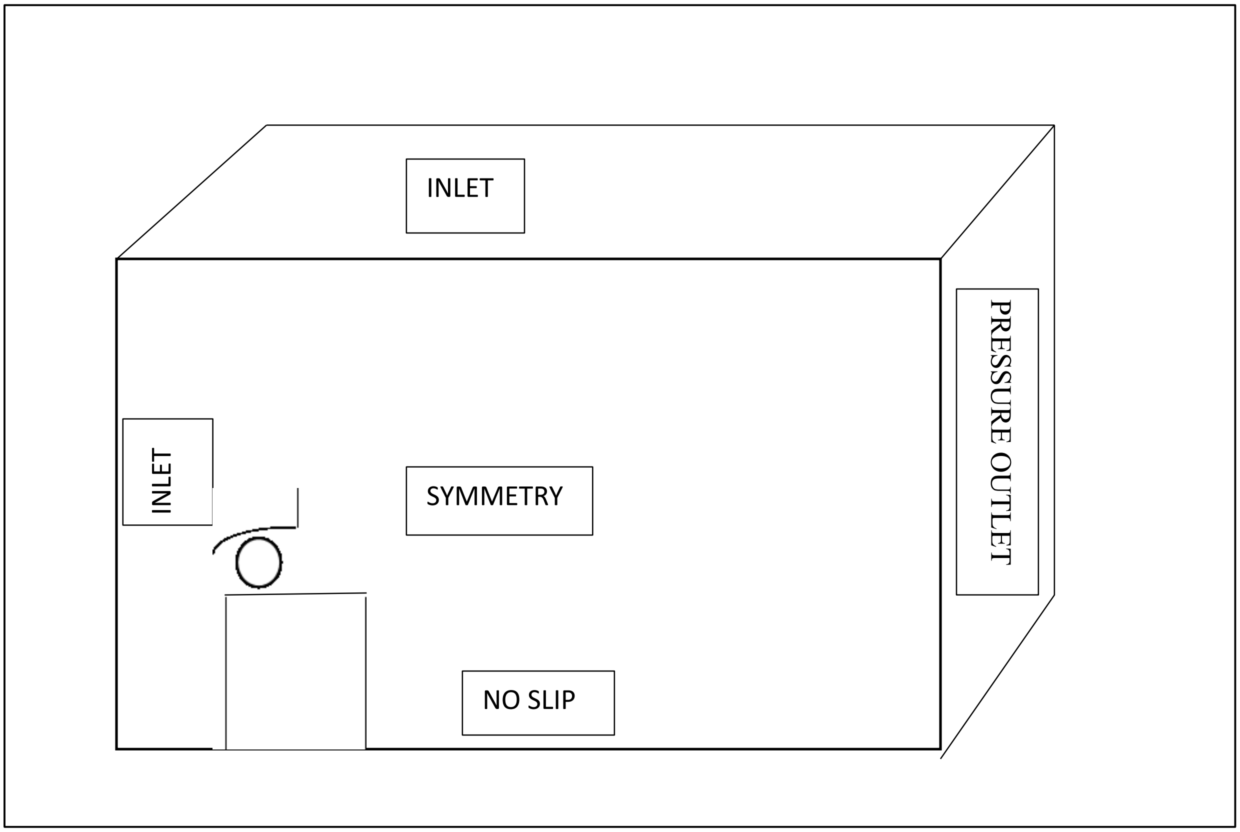

Figure 2.6: Schematic showing the boundary conditions for the computational domain

2.6.2. PHYSICAL PROPERTIES OF THE WORKING FLUID

The working fluid in this simulation is air. The specification of this working fluid are given in Table 2.1.

Properties	**Value**
Kinematic Viscosity (ν)	$1.57x10^{-5}\frac{m^2}{s}$
Density (ρ)	$1.1774\frac{kg}{m^3}$

Table 2.1: Physical properties of the working fluid

2.6.3. SOLVER

The pressure-based solver is used which is applicable for a wide range of flow regimes from low speed incompressible flow to high-speed compressible flow. It requires less memory (storage).It also allows flexibility in the solution procedure. Further, the implicit solution approach is used as the explicit approach has a very strict limit on time step size.

2.6.4. DISCRETIZATION SCHEMES IN TIME AND SPACE

The convection terms in velocity and turbulence equations are discretized gauss scheme with first order upwind interpolation scheme. Gradients of solution variables are required in order to evaluate diffusive fluxes, velocity derivatives, and for higher-order discretization schemes. The gradients of solution variables at cell centers are determined using the Least-Squares Cell-Based approach (where the solution is assumed to vary linearly). The gradients of solution variables at faces are computed using multi-dimensional Taylor series expansion. The cell-face pressures are calculated using standard interpolation scheme, while in the case of momentum, a second order upwind scheme is used. The turbulent kinetic energy k and turbulent dissipation rate ϵ are calculated using a second order upwind scheme. A first order Euler implicit scheme is used for temporal discretization.

2.6.5. SOLUTION PARAMETERS

Pressure-velocity coupling refers to the numerical algorithm which uses a combination of continuity and momentum equations to derive an equation for pressure (or pressure correction) when using the pressure-based solver. The algorithm used for this is the Semi-

Implicit Method for Pressure-Linked Equations (SIMPLE). This is because this method has the capability of having larger time steps compared to pressure implicit splitting of operators (PISO) algorithm [14]. In fact, due to the limitation on the maximum time step, the PISO solver is computationally considered to be an expensive solver. The SIMPLE algorithm sequentially performs the following steps.

1. Boundary Conditions are set.
2. In order to calculate the intermediate velocity field, Discretized momentum equation is computed.
3. Mass fluxes at the cell faces are calculated and employed.
4. Pressure equation is computed and under-relaxation factor is applied.
5. Computed mass flux at the cell faces are corrected.
6. According to the new pressure, velocity field is corrected.
7. Boundary conditions are updated accordingly.
8. Procedure is repeated until the convergence criteria is met.

CHAPTER 3 : VERIFICATION

The examination of the spatial convergence of a simulation is a straight-forward method for determining the ordered discretization error in a CFD simulation. The method involves performing the simulation on two or more successively finer grids. The term *grid convergence study* is equivalent to the commonly used term *grid refinement study*.

As the grid is refined (grid cells become smaller and the number of cells in the flow domain increase) and the time step is refined (reduced) the spatial and temporal discretization errors, respectively, should asymptotically approaches zero, excluding computer round-off error.

One significant issue in numerical computations is what level of grid resolution is appropriate. This is a function of the flow conditions, type of analysis, geometry and other variables. One is often left to start with a grid resolution and then conduct a series of grid refinements to assess the effect of grid resolution. This is known as a grid refinement study

Roache [41] suggests a grid convergence index (GCI) to provide a consistent manner in reporting the results of grid convergence studies and perhaps provide an error band on the grid convergence of the solution. The GCI can be computed using two levels of grid; however, three levels are recommended in order to accurately estimate the order of convergence and to check that the solutions are within the asymptotic range of convergence. GCI is based on Richardson Extrapolation (RE) and is considered to be the most acceptable and recommended method for discretization error estimation.

GCI is a measure of the percentage the computed value is away from the value of the asymptotic numerical value. It indicates an error band on how far the solution is from the asymptotic value. It indicates how much the solution would change with a further refinement of the grid. A small value of GCI indicates that the computations is within the asymptotic range.

However this straightforward method is not directly applicable to our case. This is because our geometry is quite complex, with multiple blades, a rotating/moving portion of the mesh with an interface, and shroud and building that multiple vortices. Further the Roache approach was developed with the assumption that the mesh is structured. The mesh that we are using is a hybrid mesh- having structured and unstructured portions.

Thus a method is used that accounts for error due to discretization in time as well as space.

3.1 GRID CONVERGENCE

Grid convergence analysis is performed among three meshes with characteristic length h and number of elements N.

In this study, C_p is the key variable and is the objective of the numerical simulations. For this purpose, based on experience and to account for the fact that the discretization error should be differentiated from other error sources (iterative convergence errors, computer round-off etc.), the grid refinement factor

$$r = \frac{h_{coarse}}{h_{fine}}$$

Should be greater than 1.1 and the grid refinement procedure is carried out systematically.

For the case where three meshes are employed,

$$r_{21} = \frac{h_2}{h_1}$$

$$r_{32} = \frac{h_3}{h_2}$$

Where r_{21} and r_{32} are the grid refinement factors for the first-second and second-third meshes respectively

Further, three different time steps Δt are also used. All the values mentioned above are given in Table 3.1.

Characteristic	**Value**
Fine Mesh Elements N_1	9,250,000
Medium Mesh Elements N_2	8,050,000
Coarse Mesh Elements N_3	7,000,000
r_{21}	1.15
r_{32}	1.15
Δt_1	0.005
Δt_2	0.01
Δt_3	0.02

Table 3.1: Grid and time step parameters for grid verification

Each grid is simulated with each of the time steps, with the C_p being the key variable.

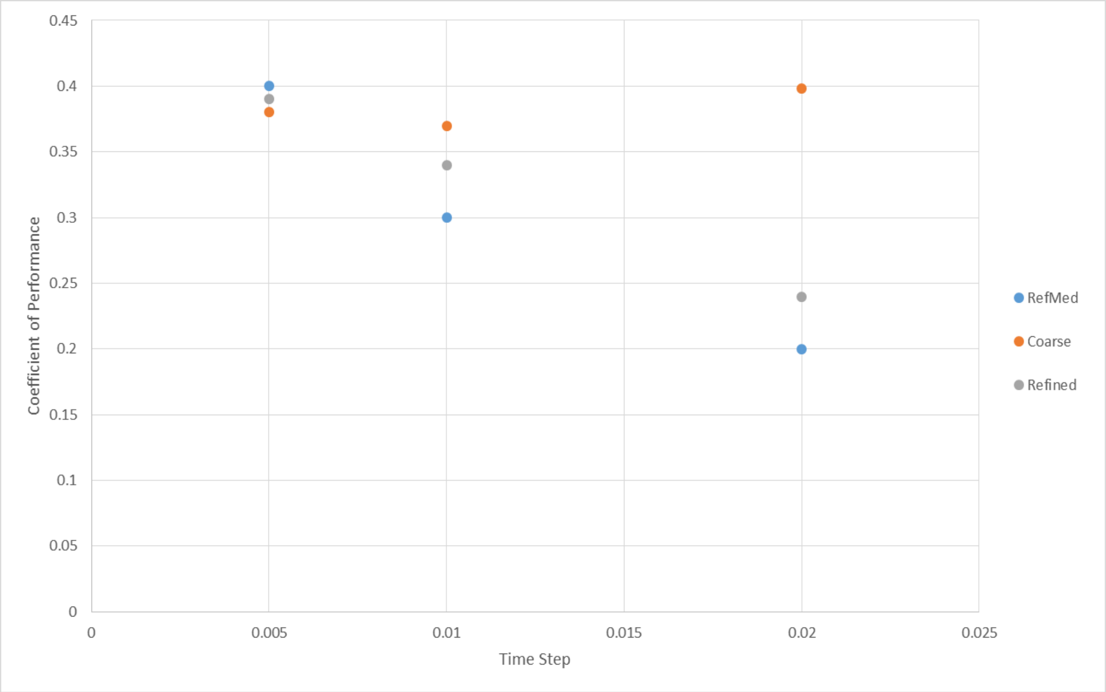

Figure 3.1: Plot of variation in C_p with time step size, for different grids

Figure 3.1 shows the results of these simulations.

As can be seen, at the finest time step (Δt_1), it is seen that all three meshes move towards a very similar value. For the case of the fine and medium meshes, the C_p increases steadily as the time step decreases and the characteristic length decreases. However this trend does not hold true for the coarse grid.

Figure 3.1 also shows us that the power prediction of the coarse grid does not vary much with change in time step. This is possibly because the mesh is too coarse to capture minute vortices or effects. However the predicted C_p is very close to the value predicted by the finest mesh at the finest time step.

Thus it is useful to establish that simulations conducted with the coarse grid at the coarse time step, are accurate enough, as this saves tremendous computational cost and time. Since the purpose of the thesis is a parametric study of the rooftop turbine, accuracy to within a certain degree is acceptable.

3.2 GRID VERIFICATION

In order to ensure that this trend (where the coarse mesh and coarse time combination provides a result that is quite close to the finest mesh and finest time step combination) presents itself ubiquitously, the same analysis was conducted for two other tip speed ratio values. Table 3.2 shows the results of these simulations.

TSR	0.45	0.5	0.6
C_p value for coarse mesh and coarse time step	0.38	0.398	0.355
C_p value for refined mesh and refined time step	0.4	0.39	0.376
% Difference between the two C_p values	5.2	-2.01	5.9

Table 3.2: C_p values for coarse and fine grids, at different tip speed ratios (TSR)

Thus, as seen in Table 3.2, there is never a difference of more than around 5% in the two values. Since this is within the range of tolerance for our design purposes, and it enables us to considerable save on computational cost, the coarse mesh and coarse time step are used for the design analysis.

CHAPTER 4 : RESULTS AND DISCUSSIONS

In this chapter, each turbine component is studied and non-dimensional parametric studies are conducted on each design parameter associated with these components, keeping the coefficient of power C_p as the key variable. The results are presented and discussed, with the optimum value for each study also being highlighted. These optimum values will be used in the next chapter to present a final design.

4.1. SHROUD

In this section, the shroud of the turbine has been presented, along with relevant analyses and discussions.

A shroud is required for the following reasons :

1. To protect the turbine from external hazards and from damage against broken blades
2. To accelerate the flow. It can serve the purpose of acting as a diffuser, thus sucking in more streamlines of flow. This has the net effect of increasing the velocity of flow inside the turbine casing.
3. To reduce noise as vortices generated by blade tips are considerably suppressed through the interference with the boundary layer within the diffuser shroud [42] [43].
4. To provide a potential surface to place solar photo-voltaic panels, if required.

Among these, the most relevant concern for the purpose of our analysis is the accelerating/flow concentrating potential of the shroud.

4.1.1. FLANGED DIFFUSER

The total power available in the wind is calculated as follows.

$$P = \frac{1}{2}\rho A v^3 \tag{4.1}$$

Thus the wind power available is directly proportional the cube of the wind speed. This shows that it is indeed substantially beneficial to try accelerating the flow with some mechanism just before it reaches the turbine [44]. It has been shown that a diffuser shaped structure is able to increase the wind speed, relevant to wind turbines [45].

A long type diffuser is ideal, as there is more acceleration of the wind speed near the entrance of the diffuser. However, a long heavy structure is not preferable in the practical sense. [32] discusses the use of a ring-type plate or “brim” at the exit periphery of a short diffuser. The brim forms vertices behind it and generates a low-pressure region behind the diffuser. Accordingly, the wind flows into a low-pressure region, the wind velocity is accelerated further near the entrance of the diffuser. It is claimed that a significant increase in the output of the wind turbine can be obtained (approximately 4-5 times) if a relatively long diffuser is used ($L_t = 1.47D$).

However the above study was conducted for a free horizontal axis wind turbine. The design of the brimmed diffuser cannot be directly applied to the shroud in our case because of two reasons :

1. The wind turbine in this case is a roof mounted wind turbine. So there cannot be flow under the shroud, as the shroud is connected to a building.

2. The turbine being used is effectively a Savonius turbine, with no overlap region. This Savonius turbine is rotated about a horizontal axis.

Clearly there is a need to redesign the shroud to account for these factors. However the goal is to leverage the concept of the generation of a low pressure region due to strong vortex formation behind a flange (which will function similar to the aforementioned brim). This low pressure region will draw more mass flow of air into the wind turbine inside the shroud.

4.1.2. DESIGN VALIDATION OF FLANGE CONCEPT

According to [32], the accelerating effect of the diffuser shroud is unaffected as long as the boundary layer flow along the inside wall of the diffuser shroud, does not show large separation. Thus two main points were considered while designing the flanged diffuser shroud, to avoid separation from occurring.

1. The entry portion of the flanged diffuser shroud has to follow the streamline flow.
2. The walls of the downwind portion (past the entry region) of the shroud are kept straight.

While these design constraints may not be optimal, they are adhered to in order to minimize the chances of flow separation.

A validation study is conducted to ensure the accelerating/flow-concentrating nature of a flanged diffuser shroud of this type. For this study, the geometry used is only the shroud on top of the building, without the turbine as shown in Figures 4.1 and 4.2.

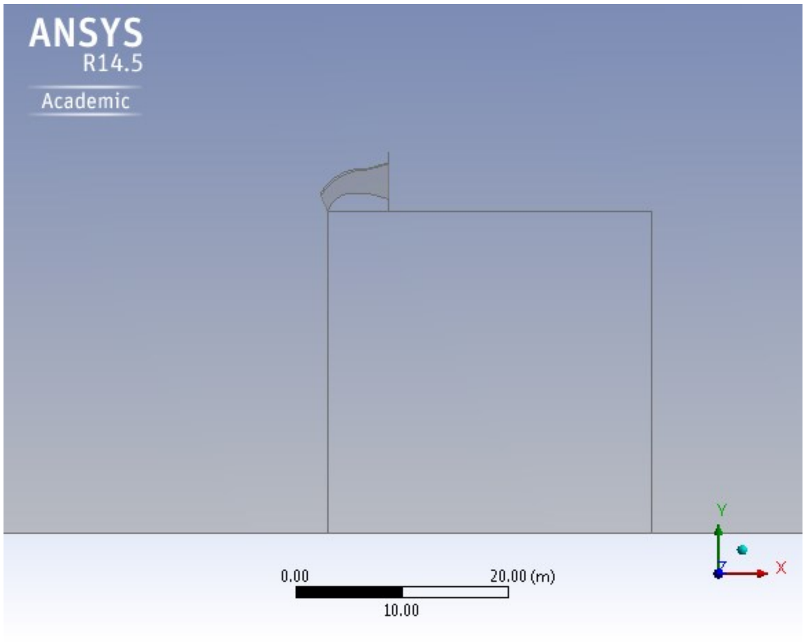

Figure 4.1: Side view of geometry of shroud on top of building

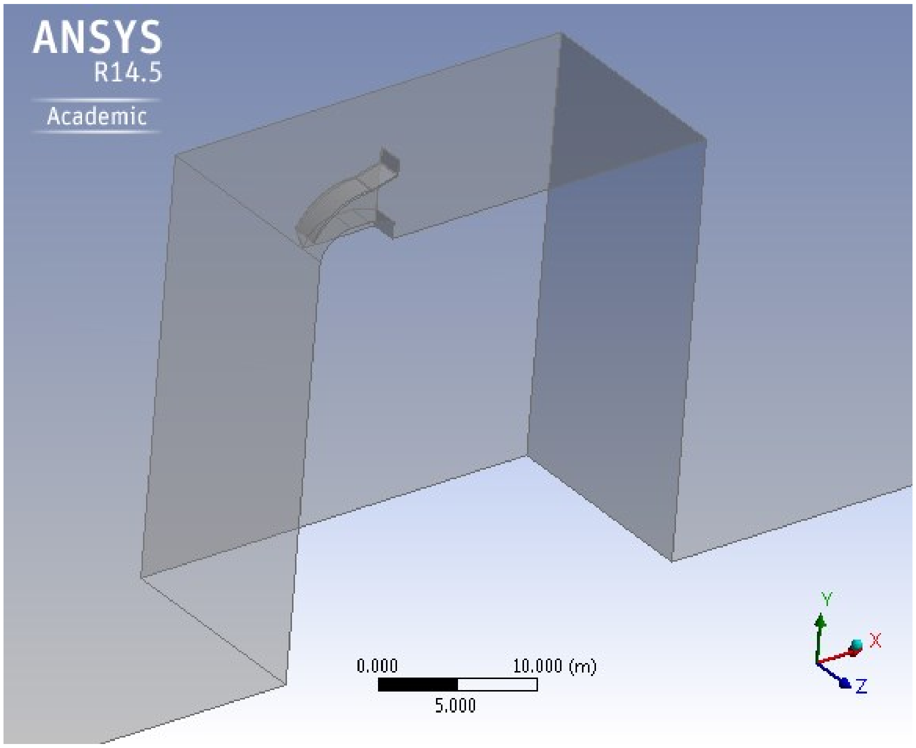

Figure 4.2: Isometric view of geometry of shroud on top of building

In this study, θ_{diff} is the angle that the floor and ceiling of the downwind portion of the flanged diffuser makes to the horizontal, as shown in Figure 4.3.

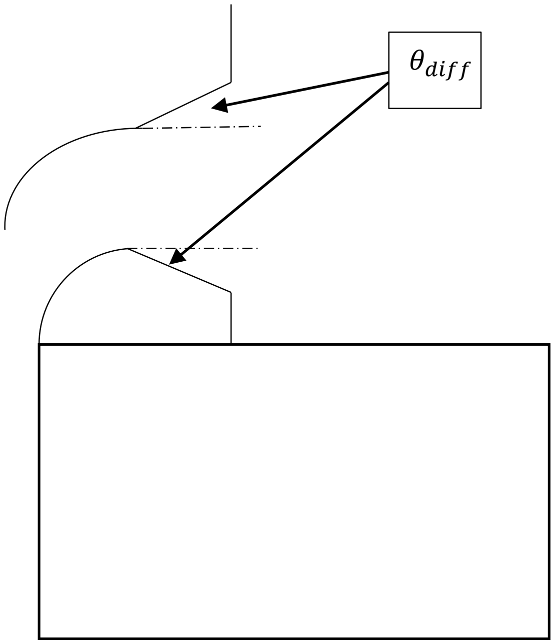

Figure 4.3: Schematic showing the flanged diffuser on top of the building, with θ_{diff} being the angle between the ceiling and floors to the horizontal respectively.

This angle, θ_{diff} is increased from 0° to 15° in increments of 5°, and the maximum velocity inside the diffuser shroud is monitored. The results of this study are presented in Figure 4.4. While an atmospheric boundary layer profile is used as inlet boundary condition, the free stream velocity of the wind at the height of the turbine is $6\frac{m}{s}$ at the height of the turbine.

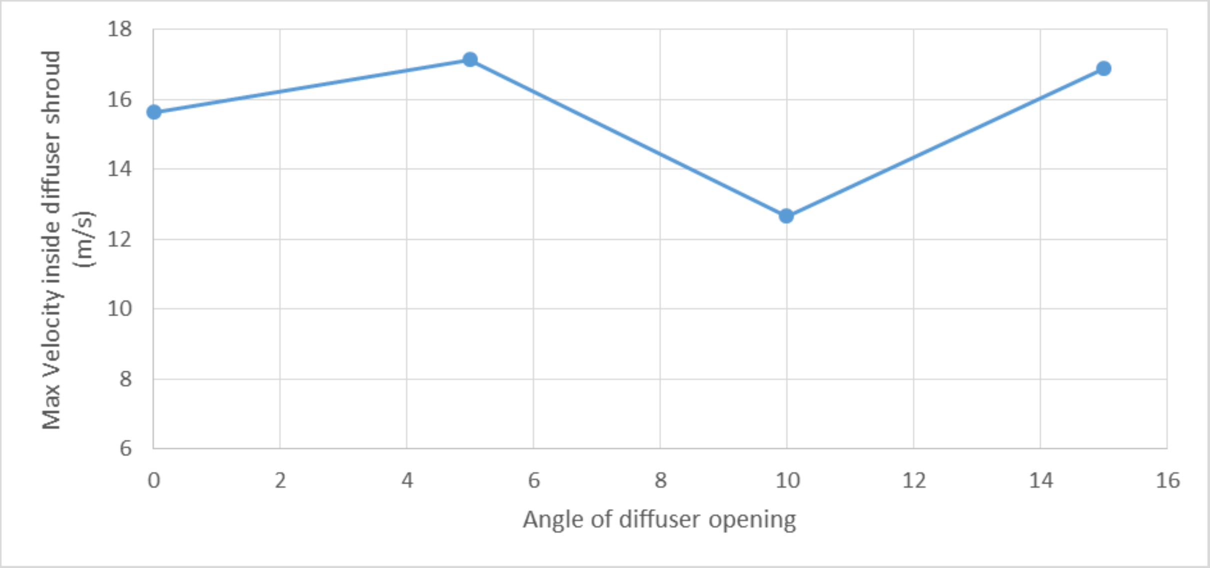

Figure 4.4: Variation of max velocity inside diffuser shroud with θ_{diff}

The instantaneous velocity streamlines for each of these cases are shown in Figures 4.5 through 4.8.

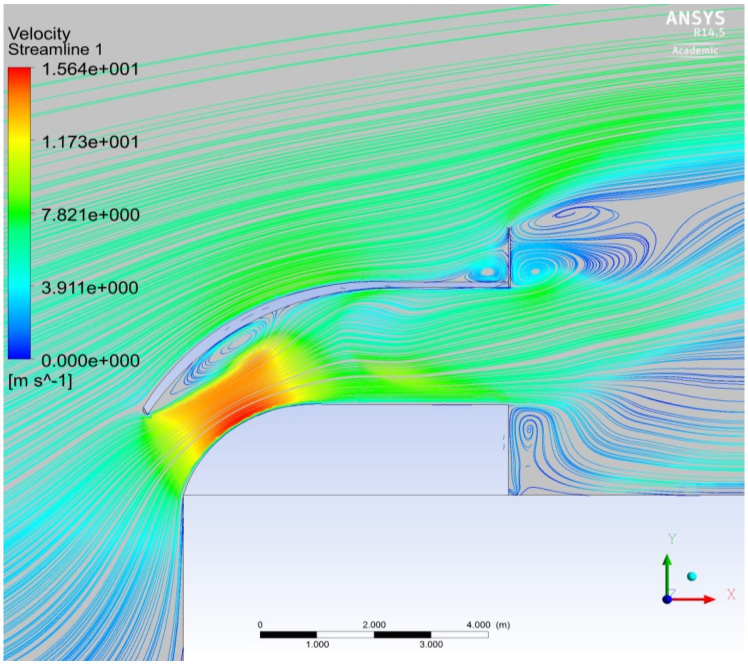

Figure 4.5: Instantaneous velocity streamlines for $\theta_{diff} = 0°$

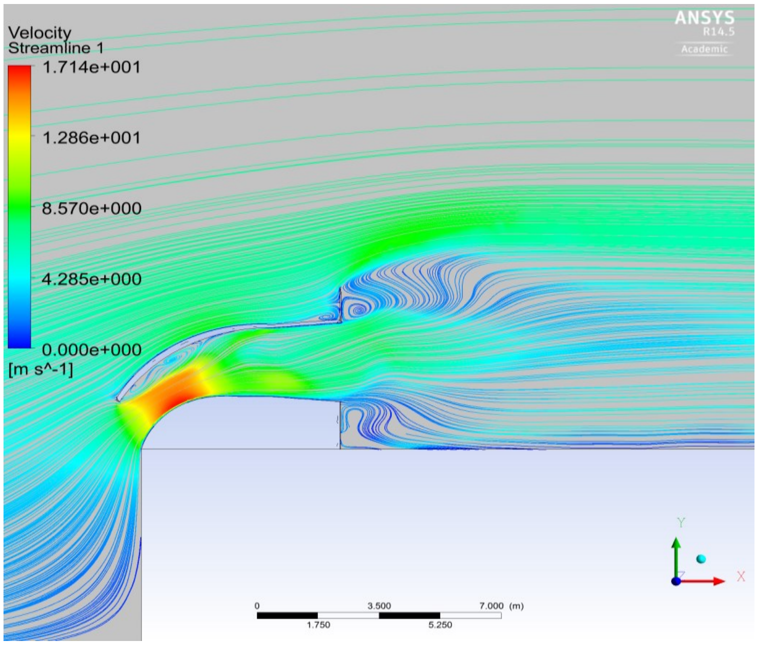

Figure 4.6: Instantaneous velocity streamlines for $\theta_{diff} = 5°$

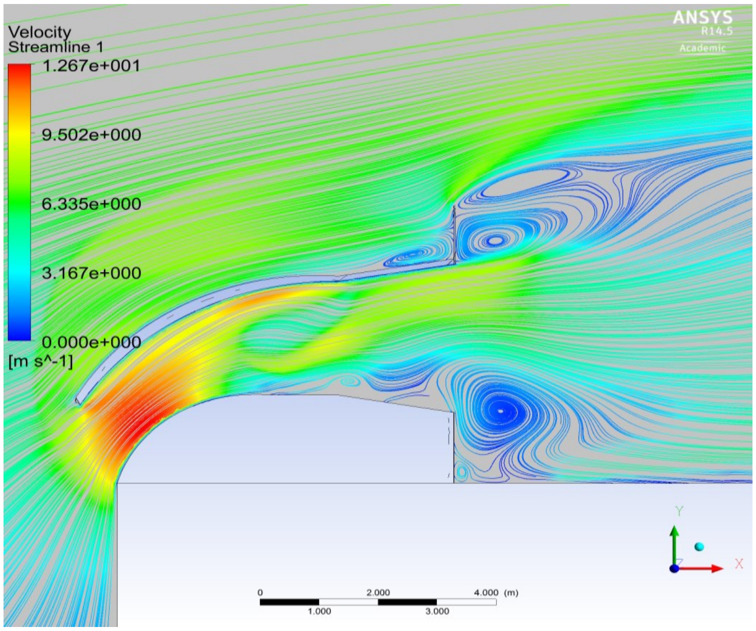

Figure 4.7: Instantaneous velocity streamlines for $\theta_{diff} = 10°$

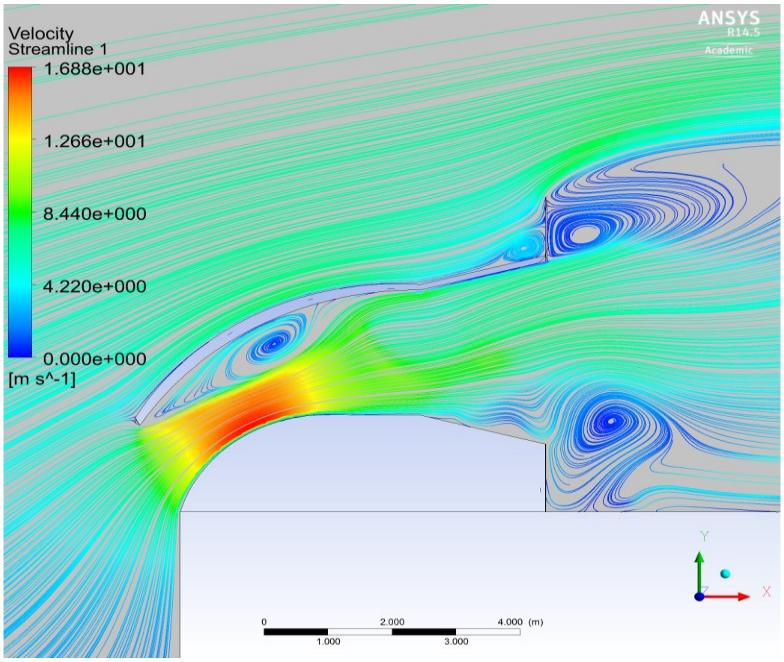

Figure 4.8: Instantaneous velocity streamlines for $\theta_{diff} = 15°$

From Figures 4.5 through 4.8, it is clear that the flanged diffuser shroud is capable of concentrating the flow and increasing the wind speed substantially (between 2-3 times). This fact is extremely important as it is the foundation for the remaining studies discussed in this chapter. Further, the maximum acceleration of the flow was obtained for the diffuser shroud having an angle of 5°. Thus a slight incline in the floor and ceiling of the downwind portion of the flanged diffuser is clearly beneficial. In the remaining studies described in this chapter, θ_{diff} has been maintained at a value of zero, for the sake of simplicity.

4.1.3. STUDY OF HEIGHT OF FLANGE

The correct size of the vortex formed behind the flange is vital. This is because the low pressure region due to this vortex formation is directly responsible for the increase in mass flow of wind into the turbine. The height of the flange decides the size of the vortex behind the flange. However a larger vortex does not necessarily mean more accelerated flow, or better performance of the turbine.

A study is conducted to monitor the effect of change in height of the flange h, upon the output performance of the turbine C_p. The height of the shroud from the building H is $2.74\ m$. Five different set-ups were used for the purpose of analysis. For this analysis, the tip speed ratio, $\lambda = 0.5$ and free stream velocity of wind at the height of the turbine is $v_\infty = 3.89 \frac{m}{s}$.

Figure 4.9 shows a schematic of the flanged diffuser shroud used for this study, with relevant parameters labelled.

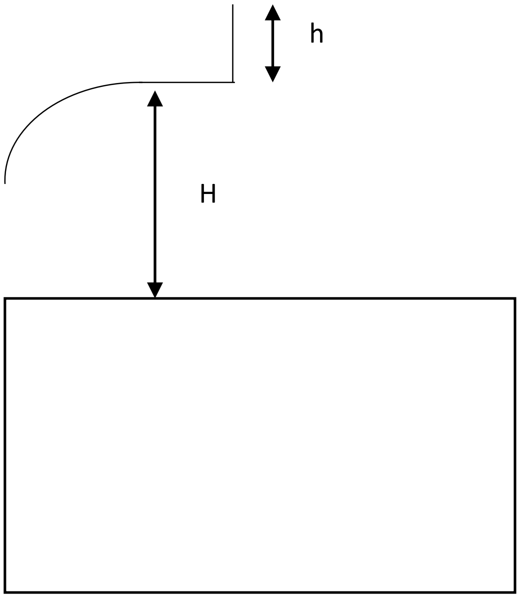

Figure 4.9: Schematic showing the flanged diffuser on top of the building, with h being the height of the flange and H being the height of the shroud from the building

Table 4.1 shows the flange height h and height ratio $\frac{h}{H}$ of each set up.

Configuration	Height of flange h (m)	Height ratio $\frac{h}{H}$
1	0.548	0.2
2	0.748	0.273
3	1	0.365
4	1.37	0.5

Table 4.1: Height of flange h and height ratio $\frac{h}{H}$ for each configuration

Figures 4.10 through 4.13 show the instantaneous velocity streamlines for each set up. The vortex formed behind the flange is seen vividly and has been highlighted in Figure 4.11. Furthermore, Figure 4.14 presents the variation of turbine output performance C_p with the height ratio $\frac{h}{H}$, and finds the optimal height ratio $\frac{h}{H}_{opt} = 0.273$ for this particular turbine.

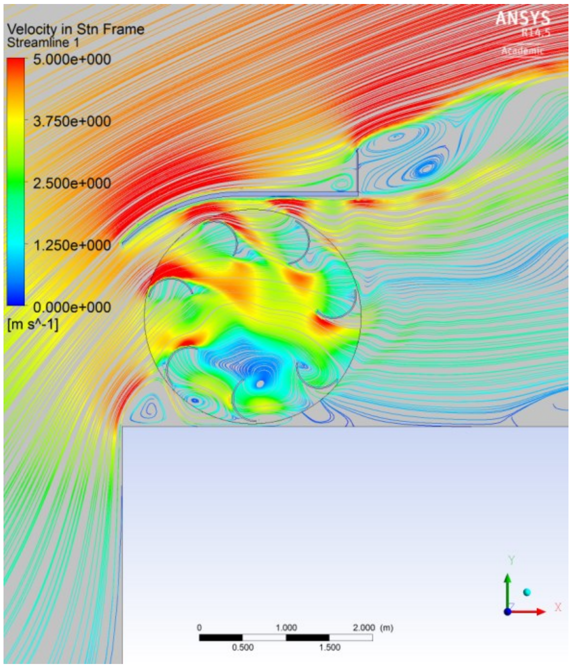

Figure 4.10: Instantaneous velocity streamlines for $\frac{h}{H} = 0.2$

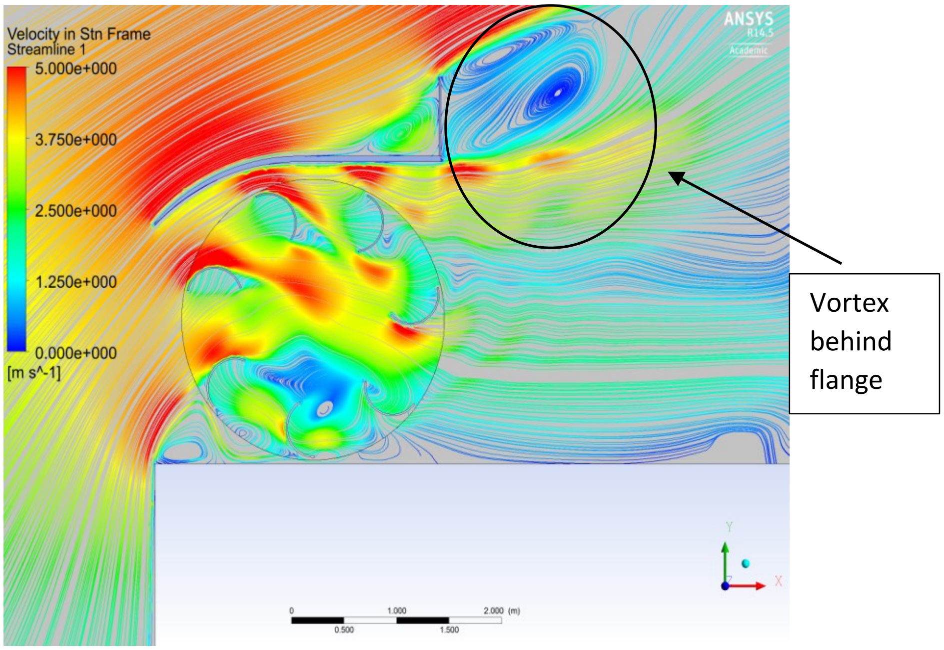

Vortex behind flange

Figure 4.11: Instantaneous velocity streamlines for $\frac{h}{H} = 0.273$

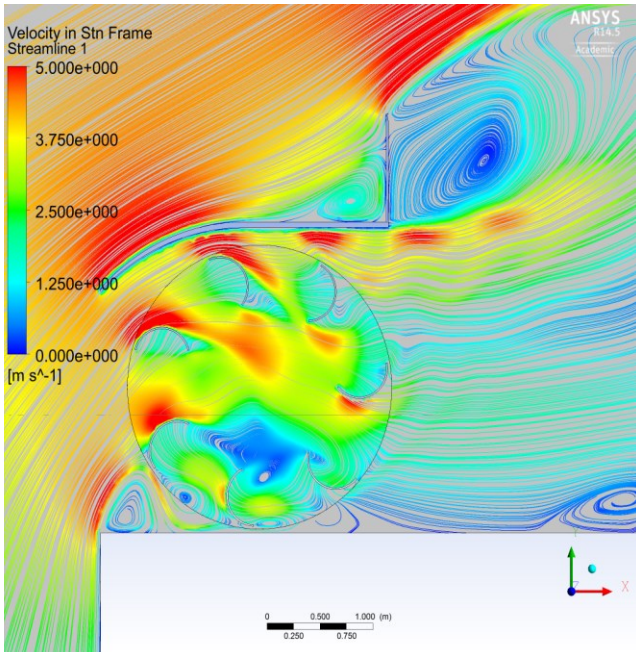

Figure 4.12: Instantaneous velocity streamlines for $\frac{h}{H} = 0.365$

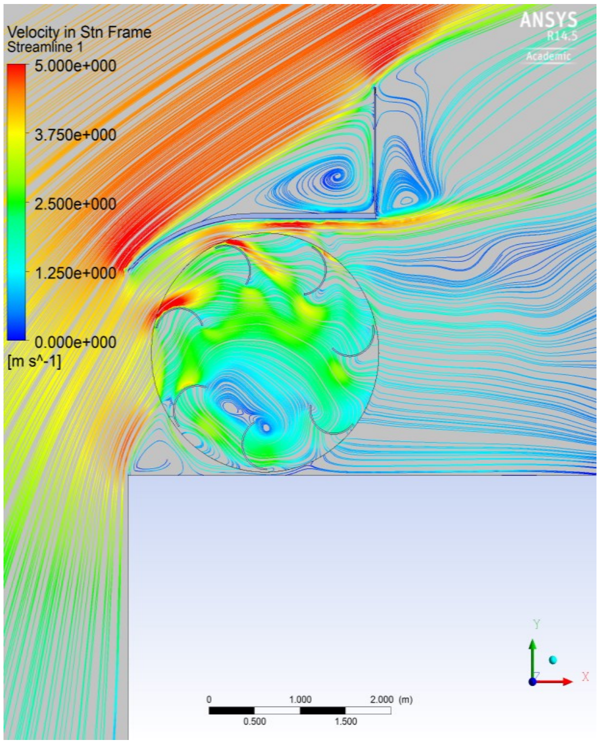

Figure 4.13: Instantaneous velocity streamlines for $\frac{h}{H} = 0.5$

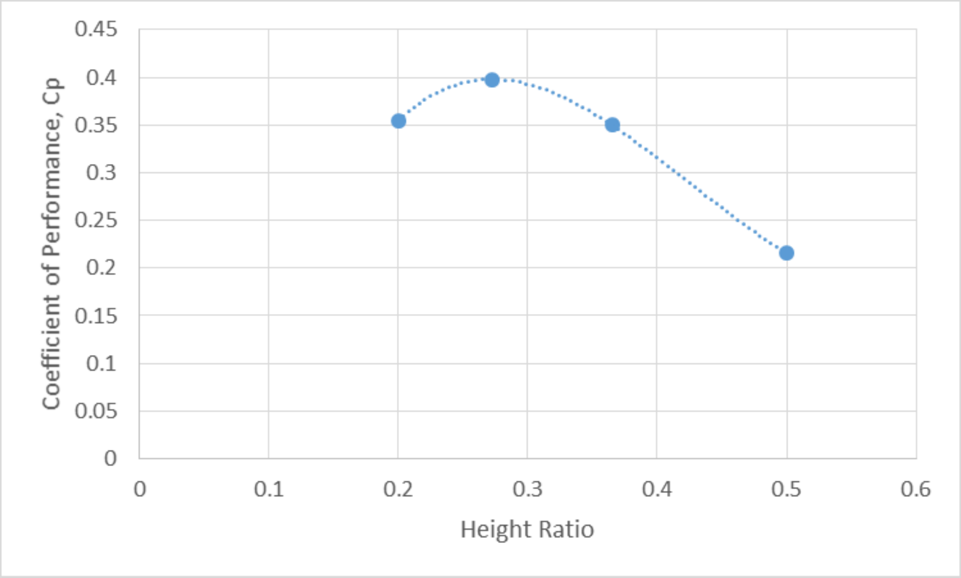

Figure 4.14: Plot showing variation of C_p with height ratio, $\frac{h}{H}$

4.1.4. STARTING POINT OF SHROUD

It is desirable to capture and concentrate as much flow as possible into the turbine, without allowing flow separation to occur. However, extending the shroud much ahead of the building does not guarantee more capture of flow, and indeed, could affect the concentration of the flow negatively. A study is conducted to find the effect of change in the distance y of the entry point of the shroud from the edge of the building, upon the output performance C_p of the turbine. The length of the ramp in front of the turbine is $Y = 1.143\,m$. Three different setups were used. For this analysis, the tip speed ratio, $\lambda = 0.6$ and free stream velocity of wind at the height of the turbine is $v_\infty = 3.89\frac{m}{s}$.

Figure 4.15 shows a schematic of the flanged diffuser shroud used for this study, with relevant parameters labelled.

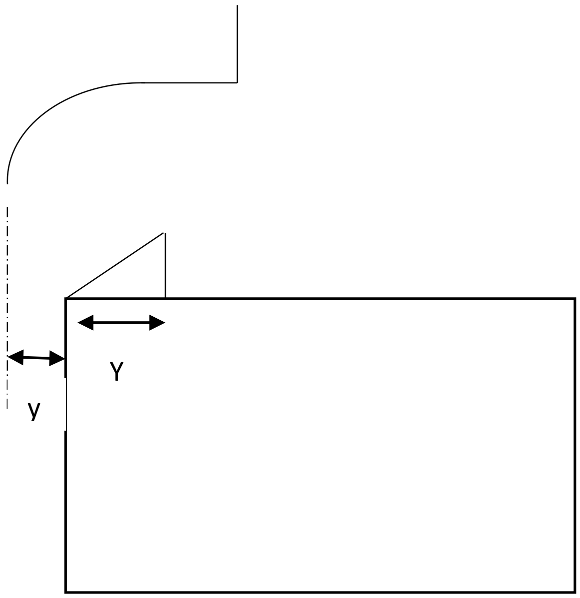

Figure 4.15: Schematic showing the flanged diffuser on top of building, with y being the horizontal displacement of starting point of shroud from the building, and Y being the length of the ramp

Table 4.2 shows the distance of entry point of shroud from edge of building y and the ratio of this distance to the length of the ramp $\frac{y}{Y}$ for each set up.

Configuration	**Distance of entry point of shroud from building edge y (m)**	$\frac{\boldsymbol{y}}{\boldsymbol{Y}}$
1	0.5715	0.5
2	0	0
3	-0.5715	-0.5

Table 4.2: Horizontal displacement of shroud entry point y and ratio $\frac{y}{Y}$ for each configuration

Figures 4.16 through 4.18 show the instantaneous velocity streamlines for each set up. Furthermore, Figure 4.19 presents the variation of turbine output performance C_p with the ratio $\frac{y}{Y}$, and finds the optimal ratio $\frac{y}{Y}_{opt} = 0$ for this particular turbine.

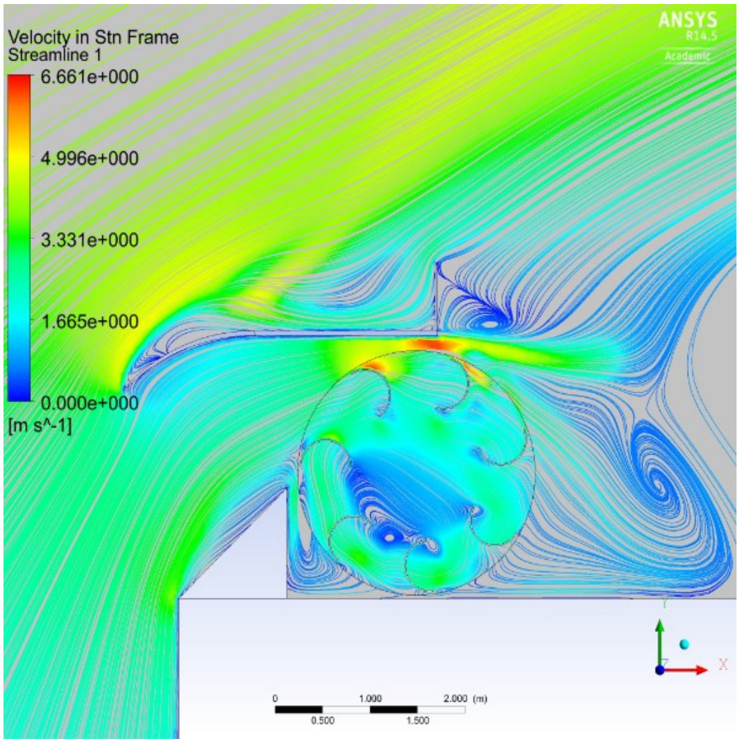

Figure 4.16: Instantaneous velocity streamlines for $\frac{y}{Y} = 0.5$

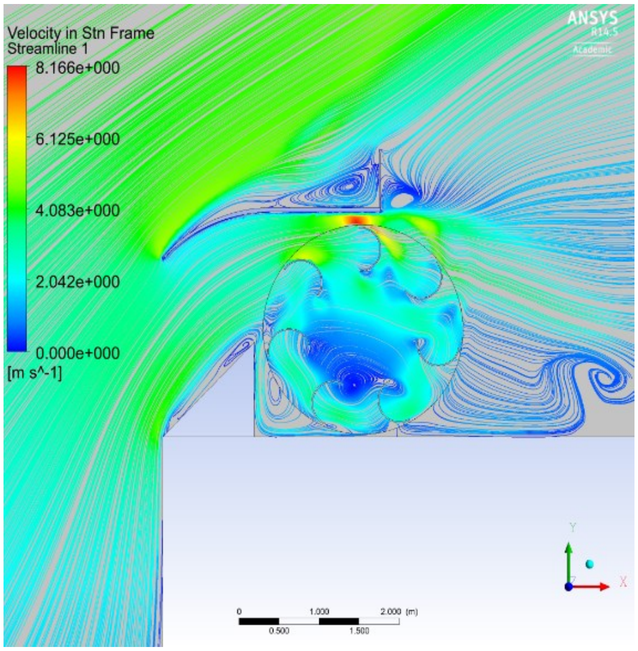

Figure 4.17: Instantaneous velocity streamlines for $\frac{y}{Y} = 0$

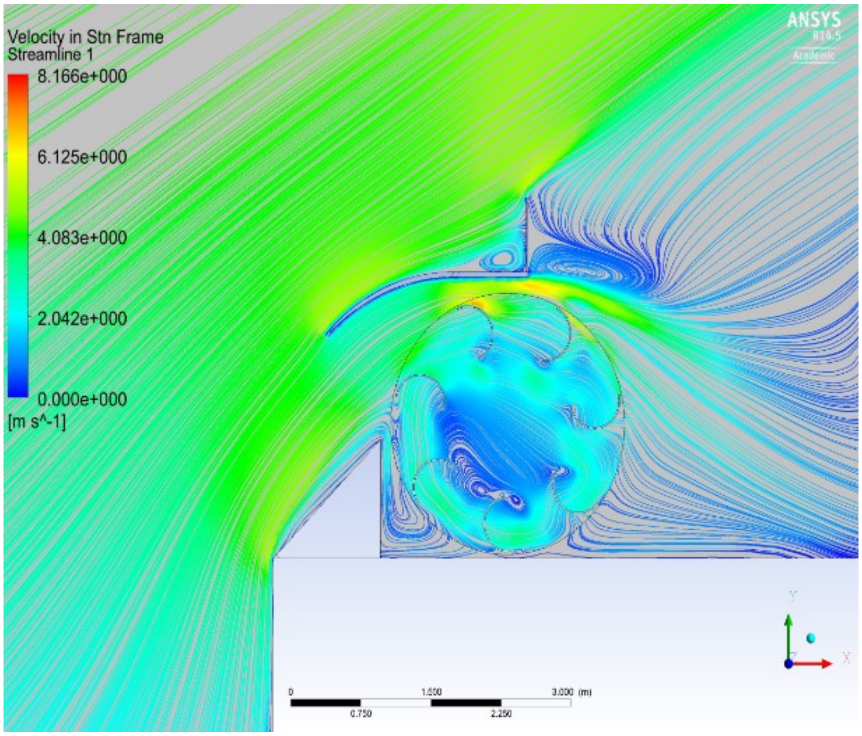

Figure 4.18: Instantaneous velocity streamlines for $\frac{y}{Y} = -0.5$

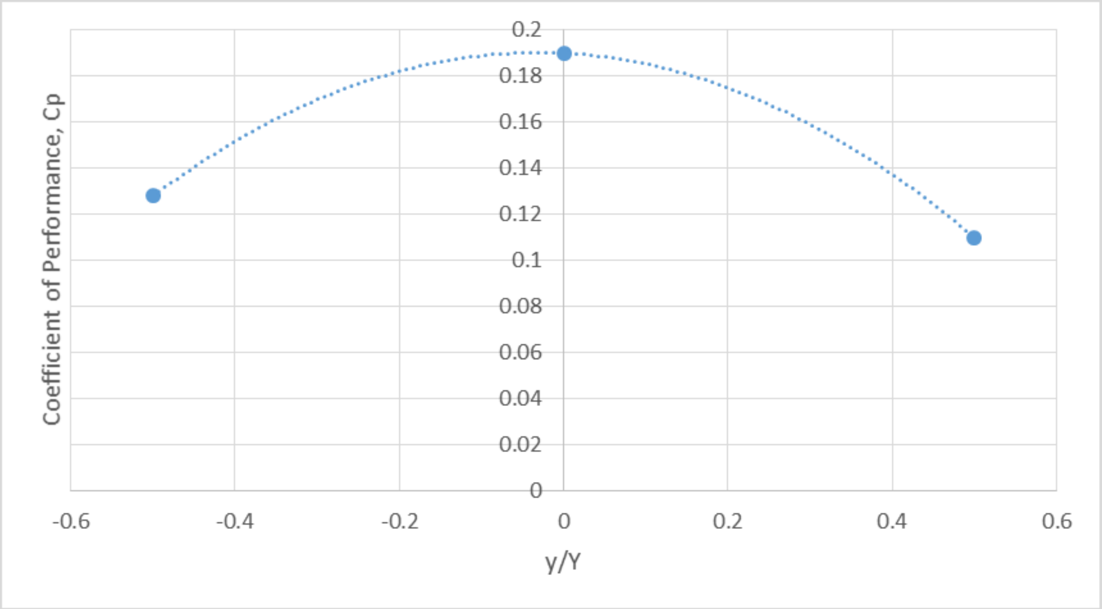

Figure 4.19: Plot showing variation of C_p with change in $\frac{y}{Y}$

4.1.5. LENGTH OF SHROUD

The length of the shroud along the direction of flow of wind is another very important parameter. An increase in length need not necessarily lead to an increase in the mass flow of wind entering the turbine, since the floor and ceiling of the shroud are horizontal i.e. $\theta_{diff} = 0°$.

A study is conducted to find the effect of change in the length of the shroud L upon the output performance C_p of the turbine. The height of the shroud above the building $H = 2.74\,m$. Four different setups were used. For this analysis, the tip speed ratio, $\lambda = 0.5$ and free stream velocity of wind at the height of the turbine is $v_\infty = 3.89\frac{m}{s}$.

Figure 4.20 shows a schematic of the flanged diffuser shroud used for this study, with relevant parameters labelled.

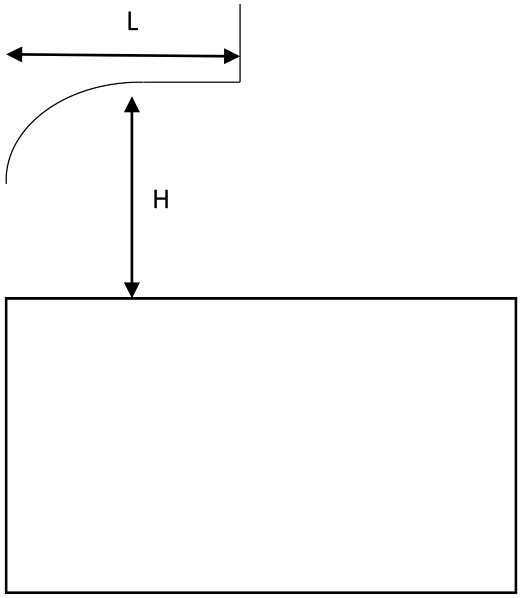

Figure 4.20: Schematic showing flanged diffuser shroud on top of building, with H being the height of the shroud from the building, and L being the length of the shroud.

Table 4.3 shows the length of the shroud L and the ratio of this distance to the height H for each set up.

Configuration	Length of shroud L (m)	$\frac{L}{H}$
1	1.37	0.5
2	2.055	0.75
3	2.74	1
4	3.425	1.25

Table 4.3: Length of shroud L and ratio to height from building, $\frac{L}{H}$ for each configuration

Figures 4.21 through 4.24 show the instantaneous velocity streamlines for each set up. Furthermore, Figure 4.25 presents the variation of turbine output performance C_p with the ratio $\frac{L}{H}$, and finds the optimal ratio $\frac{L}{H}_{opt} = 1$ for this particular turbine.

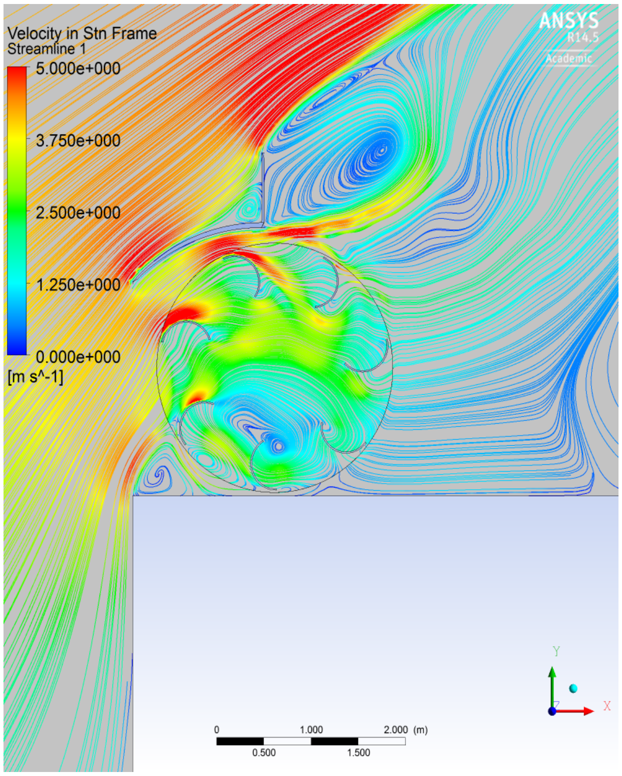

Figure 4.21: Instantaneous velocity streamlines for $\frac{L}{H} = 0.5$

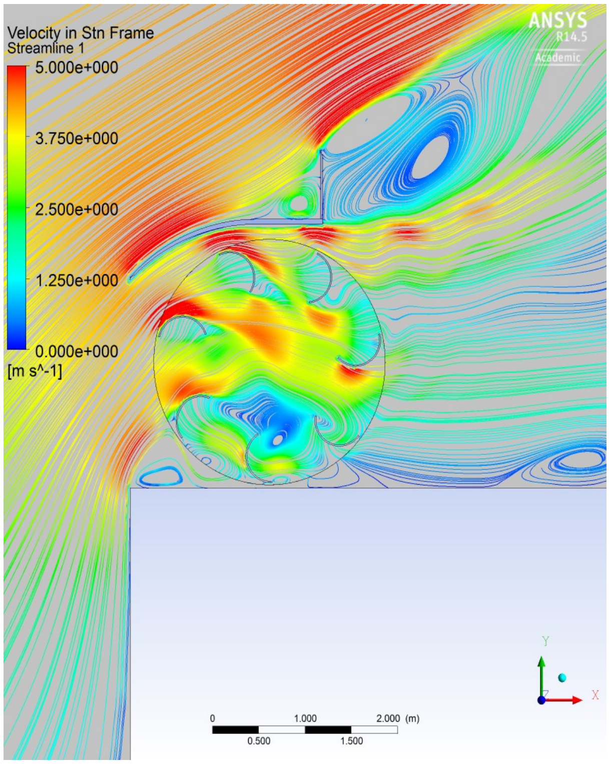

Figure 4.22: Instantaneous velocity streamlines for $\frac{L}{H} = 0.75$

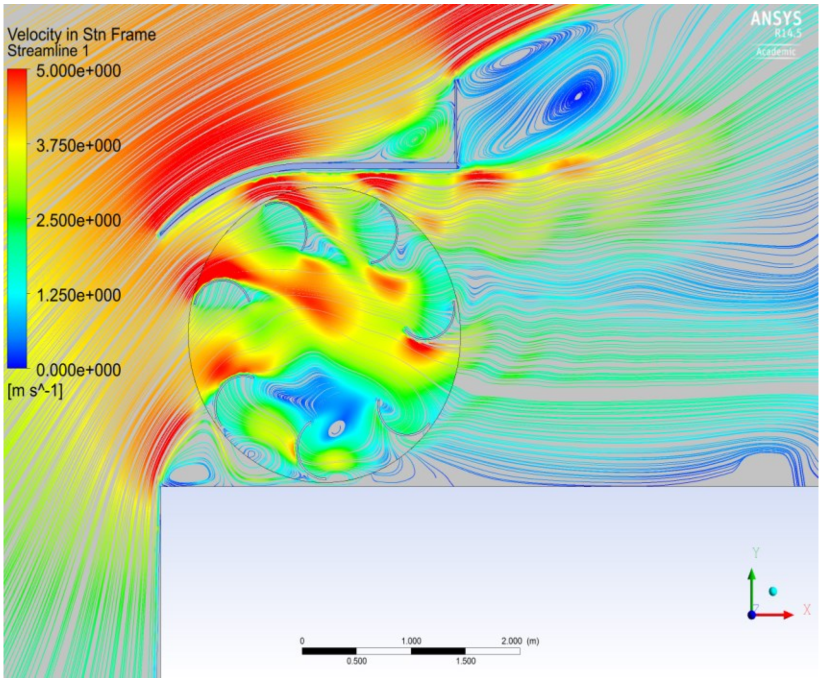

Figure 4.23: Instantaneous velocity streamlines for $\frac{L}{H} = 1.0$

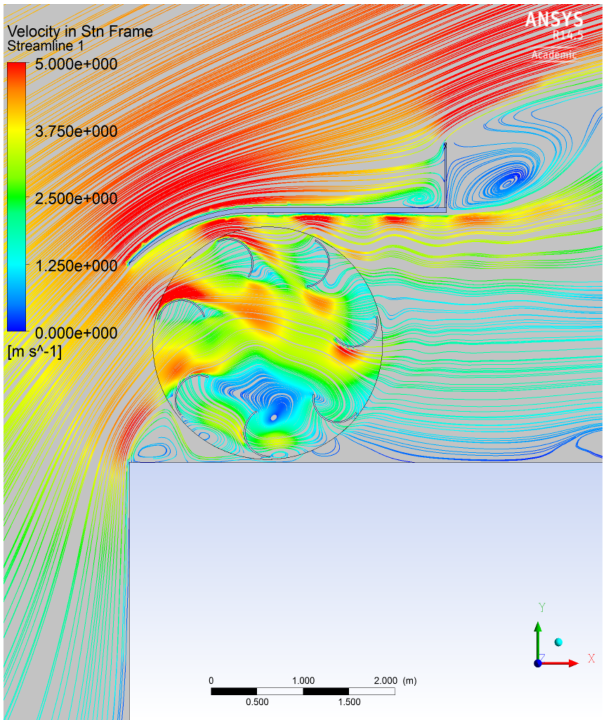

Figure 4.24: Instantaneous velocity streamlines for $\frac{L}{H} = 1.25$

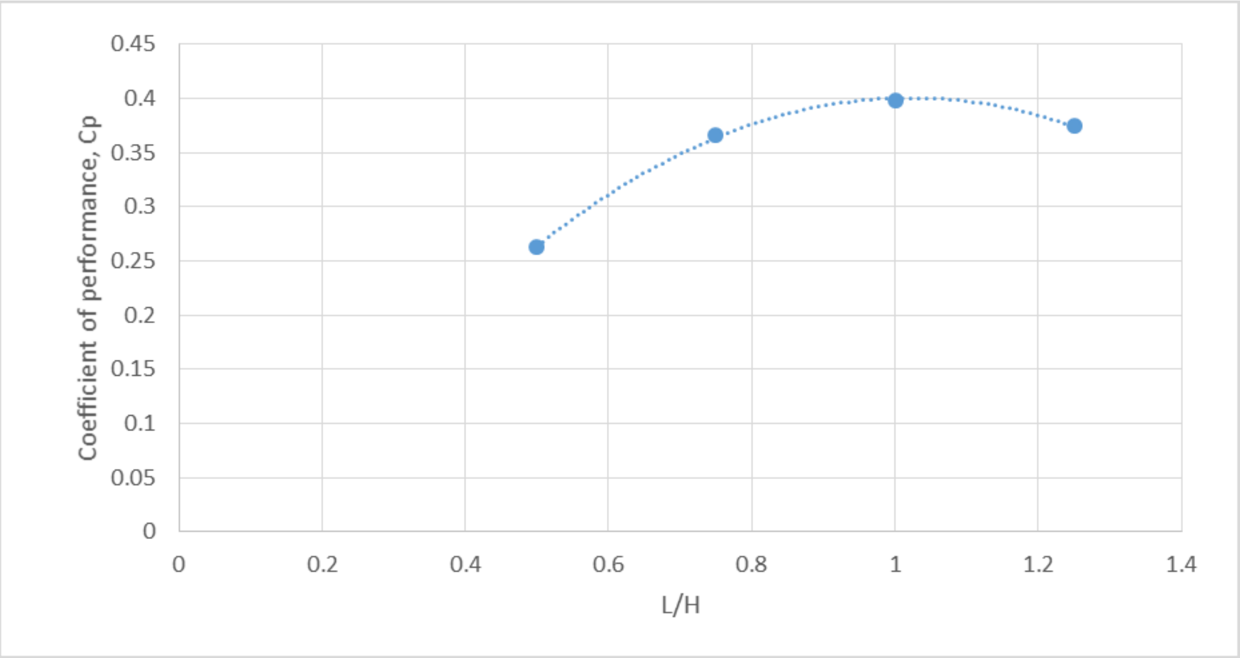

Figure 4.25: Plot showing variation of C_p with change in the ratio $\frac{L}{H}$

4.2. BLADES

This section explores the design of the turbine blades for this particular kind of turbine. It is worth noting that this design process is not trivial as we must account for the fact that the turbine is located on top of a roof, which acts as a flow concentrator. Further, the turbine is located inside a shroud. Thus the turbine blades have to be designed specifically for this case.

Two main parameters that are looked at for the design of the blades. These are the circumferential length of the blade and the number of blades. While it is possible that the ideal design process could be a multi-objective optimization problem with further parameters involved, such a study would be outside the scope of this thesis. This is because the motivation behind this thesis is to study how the coefficient of power varies as a certain parameter is changed, and not to find the absolute optimal design. Hence, this process has been approached by studying one parameter at a time, while keeping the other constant. It is assumed that the results of each individual optimization will be additive, and this will lead us to our final design.

4.2.1. REFERENCE POINT : STUDY OF BANKI BLADE

A turbine design similar to the one being studied is the wind turbine derived from a Banki water turbine, i.e. a turbine with a cross flow runner, proposed by Mandis et al [46]. Dragomirescu [47] studied this design to find its performance in poor wind conditions (wind speeds as low as $2-3\frac{m}{s}$) and showed quite promising results for the 2D simulations carried out.

This is of relevance to the turbine being used in this study for two reasons :

1. The similarity allows for a comparison case. Further studies described in this chapter will look at changes made to the blades of the turbine, and it is quite interesting to compare the performance output of the improved turbine, with the Banki turbine.
2. In the Banki turbine, Dragomirescu [47] shows that a double interaction occurs between the air current and the runner, this double interaction being actually a characteristic of cross flow runners. The effect of this double interaction can be positive or negative, depending on the size of a vortex formed inside the cross flow runner. It is desired to replicate this same effect in the turbine being studied in this project, with the intention of a positive double interaction, and consequently increased power output.

Using the same flanged diffuser shroud, the turbine was replaced with a Banki turbine. Figures 4.26 show the schematic of the Banki turbine design. Table 4.4 shows the parameters for design of the Banki turbine, using the design process described by Dragomirescu [47].

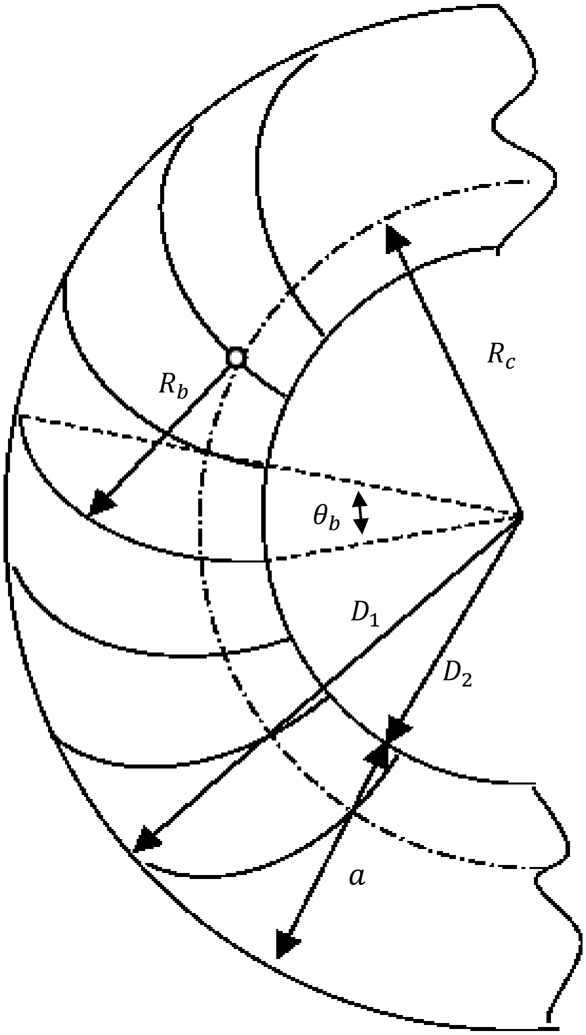

Figure 4.26: Schematic of the Banki turbine design, with relevant parameters labelled.

Property	**Symbol**	**Value**
Outer Diameter of Runner	D_1	$2.48m$
Inner Diameter of Runner	D_2	$1.6368m$
Radial rim width	a	$0.4216m$
Radius of blade	R_b	$0.40424m$

Radius of circle of centres of blades	R_c	$0.91726m$
Aperture of blade	θ_b	13.741°
Number of blades	z	26
Angle between blades	γ	13.8°

Table 4.4: Parameters for design of the Banki turbine.

For this analysis, the tip speed ratio, $\lambda = 0.38$ and free stream velocity of wind at the height of the turbine is $v_\infty = 3.89\frac{m}{s}$.

Figure 4.27 shows the instantaneous velocity streamlines for this design. The vortex formation inside the crossflow runner is easily visible, as is the double interaction of the air current with the runner blades.

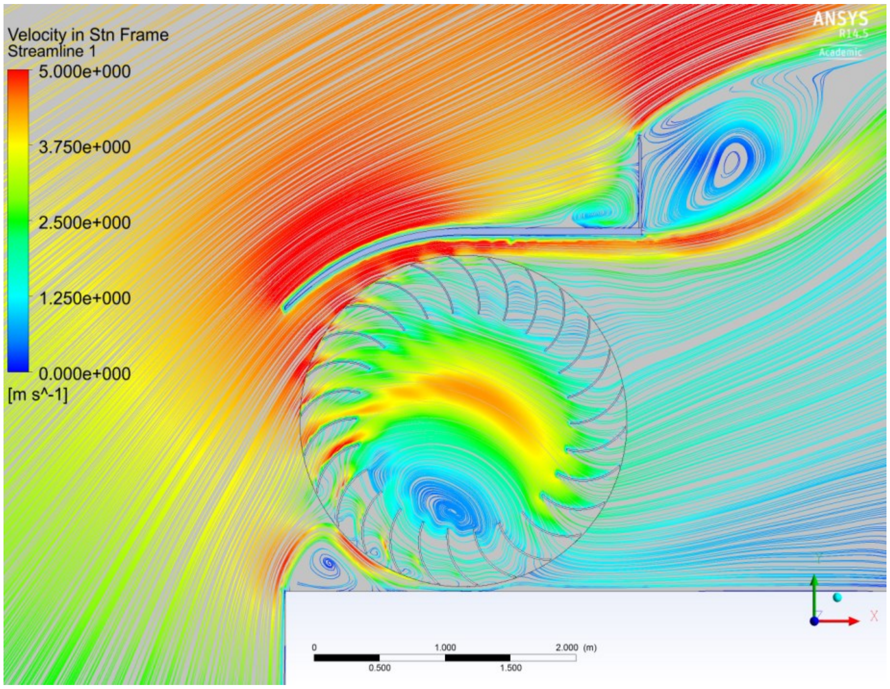

Figure 4.27: Instantaneous velocity streamlines for shrouded turbine with cross flow runner

In this case, the C_p obtained was 0.264, which serves as a reference point for future analyses.

4.2.2. STUDY OF CIRCUMFERENTIAL LENGTH OF BLADE

This study is conducted to see the effect of reducing the circumferential length of the blade, specifically by cutting a part of the trailing end of the blade (non-flow facing). Figure 4.28 shows the schematic of a blade with relevant parameters labelled. Here θ_{cut} refers to the portion of the blade that has been cut. The motivation for this study is as follows:

1. Initially a simulation is conducted with the entire blade, i.e. with $\theta_{cut} = 0°$. The instantaneous velocity contours of this case are presented in Figure 4.29. As shown in the figure, it is seen that a part of the blade is not generating power through the entire cycle. Thus this portion of the blade is non-power generating and, in fact, consumes some of the power available to the turbine, to maintain rotation.
2. It is desirable to try to create the "double interaction" effect mentioned in Section 4.2.1, that was seen in the case of the Banki turbine. This will enable the turbine to increase its power output substantially.

In this study the output performance of the turbine C_p is monitored. The radius of the blade R is 0.27 m. Five different set-ups were used for the purpose of analysis. For this analysis, the tip speed ratio, $\lambda = 0.38$ and free stream velocity of wind at the height of the turbine is $v_\infty = 3.89\frac{m}{s}$.

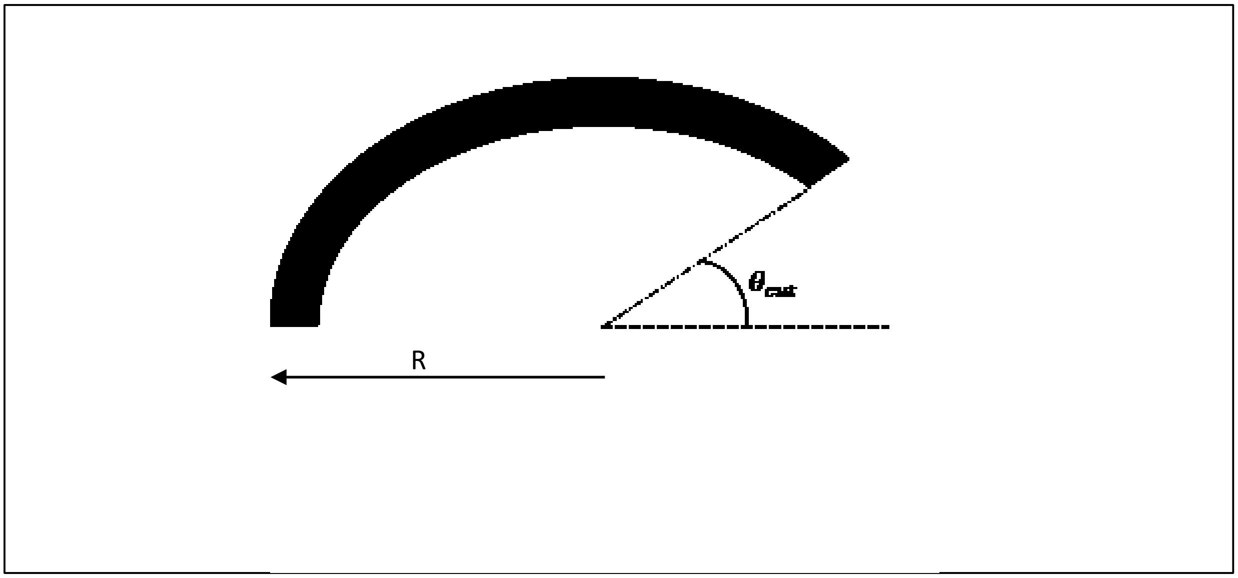

Figure 4.28: Schematic showing blade , with radius $R = 0.27m$ and θ_{cut} being the portion of the blade that has been cut.

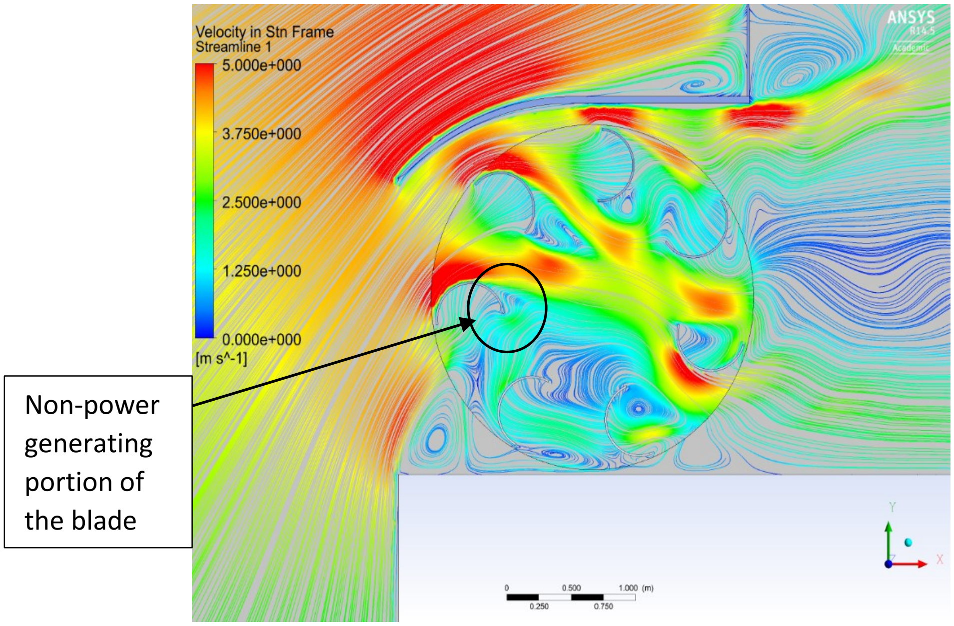

Non-power generating portion of the blade

Figure 4.29: Instantaneous velocity streamlines for $\theta_{cut} = 0°$

Table 4.5 shows the angle of cut θ_{cut} of each set up.

Setup	$\boldsymbol{\theta_{cut}}$
1	25

2	30
3	35
4	45
5	60

Table 4.5: θ_{cut} values for each of the configurations used in the study

Figures 4.30 through 4.34 show the instantaneous velocity streamlines for each set up. The double interaction effect is seen clearly for the case with $\theta_{cut} = 30°$ is seen vividly and has been highlighted in Figure 4.31.

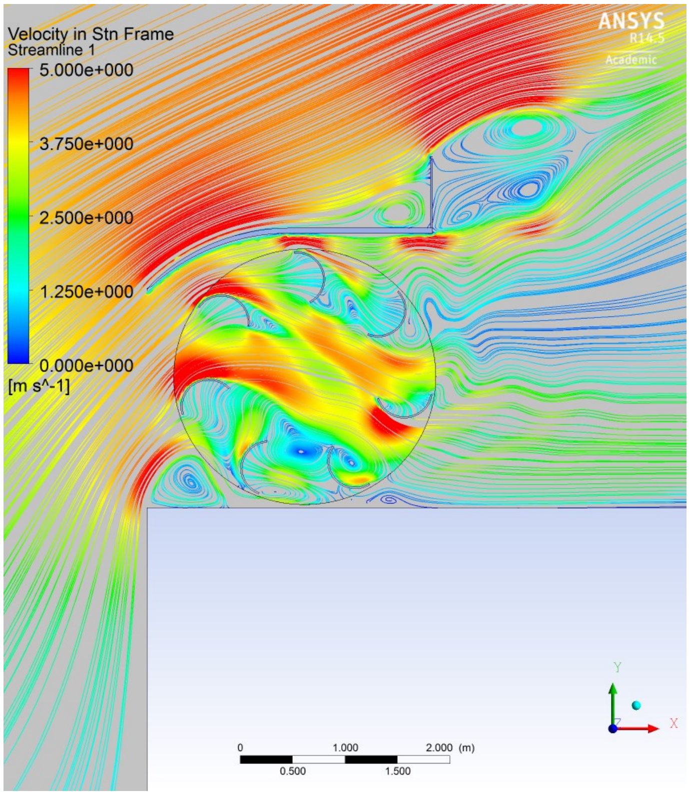

Figure 4.30: Instantaneous velocity streamlines for $\theta_{cut} = 25°$

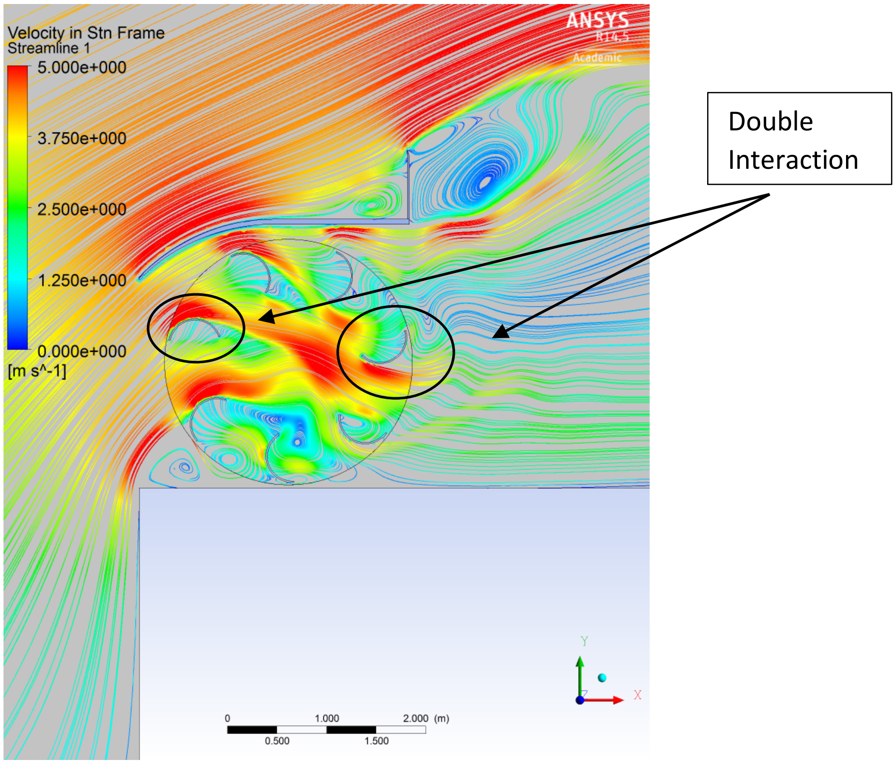

Figure 4.31: Instantaneous velocity streamlines for $\theta_{cut} = 30°$

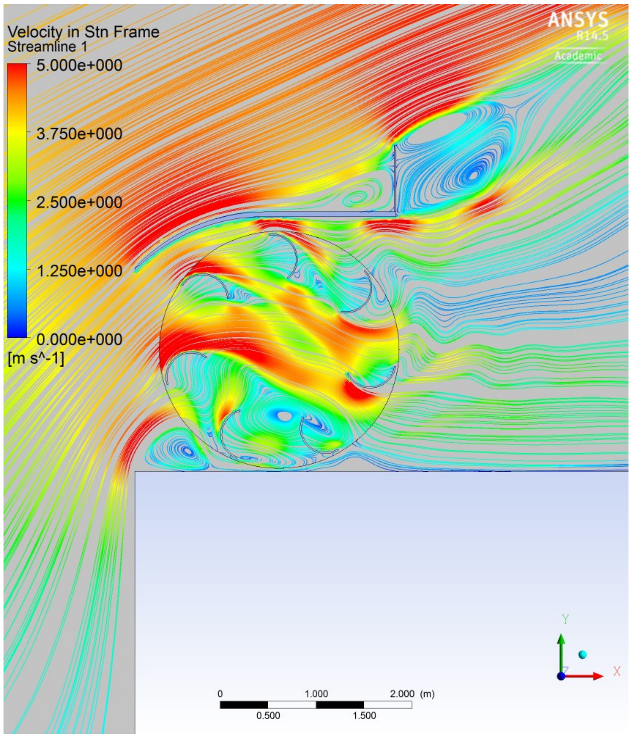

Figure 4.32: Instantaneous velocity streamlines for $\theta_{cut} = 35°$

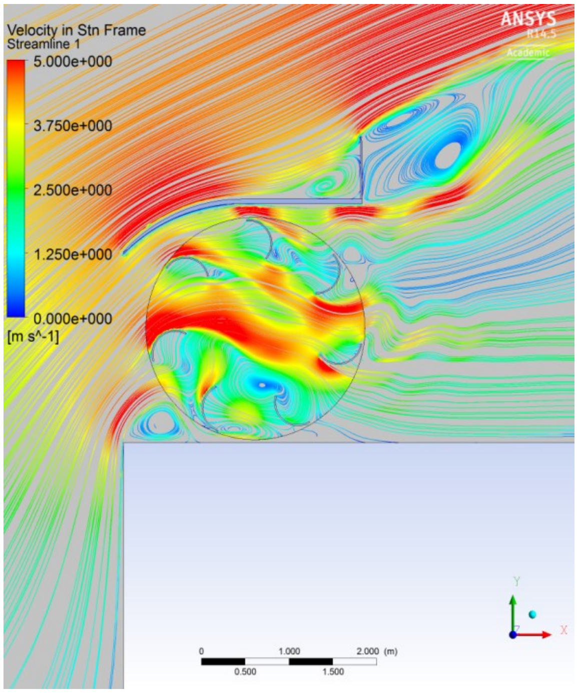

Figure 4.33: Instantaneous velocity streamlines for $\theta_{cut} = 45°$

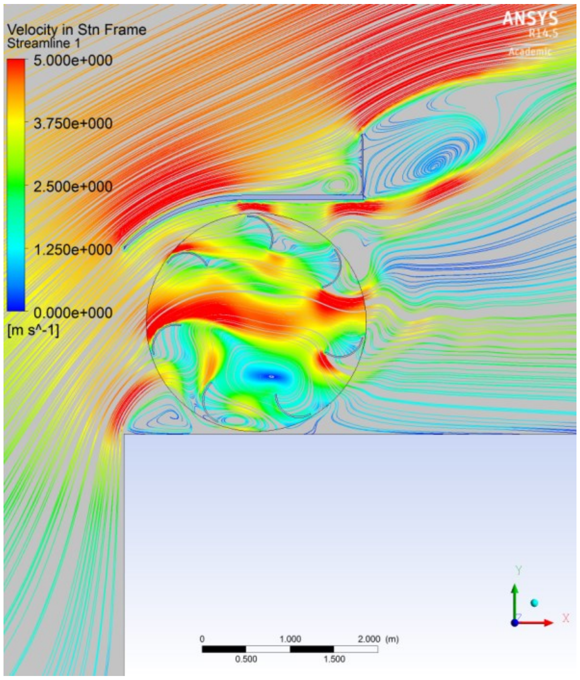

Figure 4.34: Instantaneous velocity streamlines for $\theta_{cut} = 60°$

Furthermore, Figure 4.35 presents the variation of turbine output performance C_p with the angle of cut θ_{cut}, and finds the optimal angle of cut $\theta_{cut_{opt}} = 30°$ for this particular turbine blade. The reason this design is so successful is that the flow streamlines, upon making contact with the first blade, is redirected towards the blade diametrically opposite to it. Thus at any given time, there are 4-5 power generating blades.

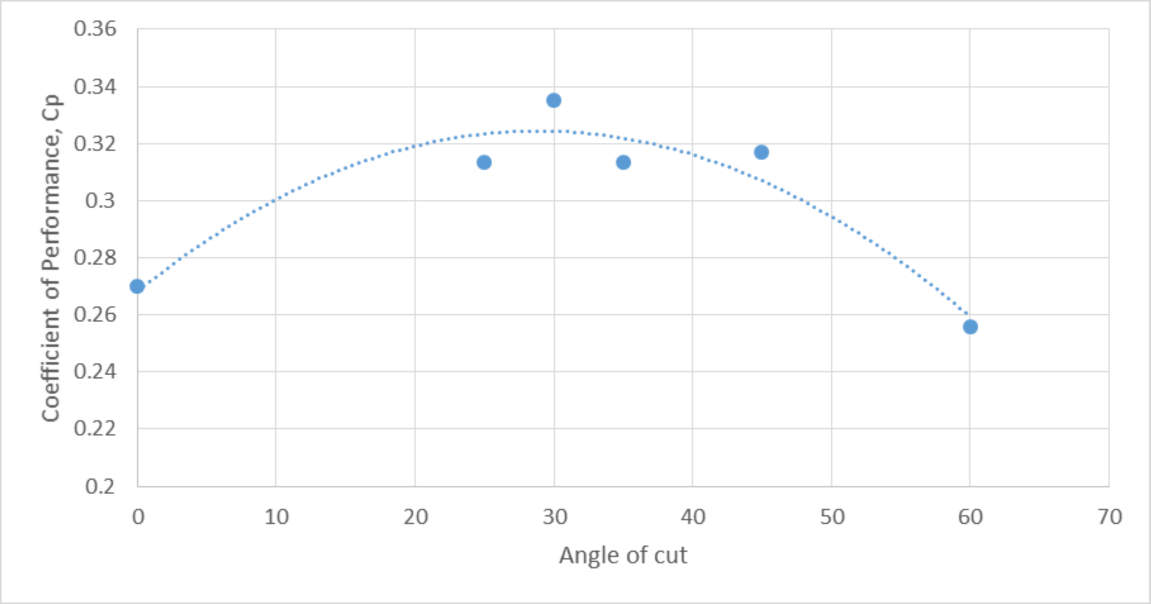

Figure 4.35: Plot showing variation of C_p with change in θ_{cut}

It is worth noting that in these cases, it is apparent that the turbine ceases to operate purely as a drag-based turbine. Figure 4.36 shows the pressure plot for the $\theta_{cut} = 30°$ case. The high and low pressure regions below and above the blade respectively, have been marked. They clearly indicates that due to the pressure difference across the blade, a lift effect acts on the blades that adds to the power generation.

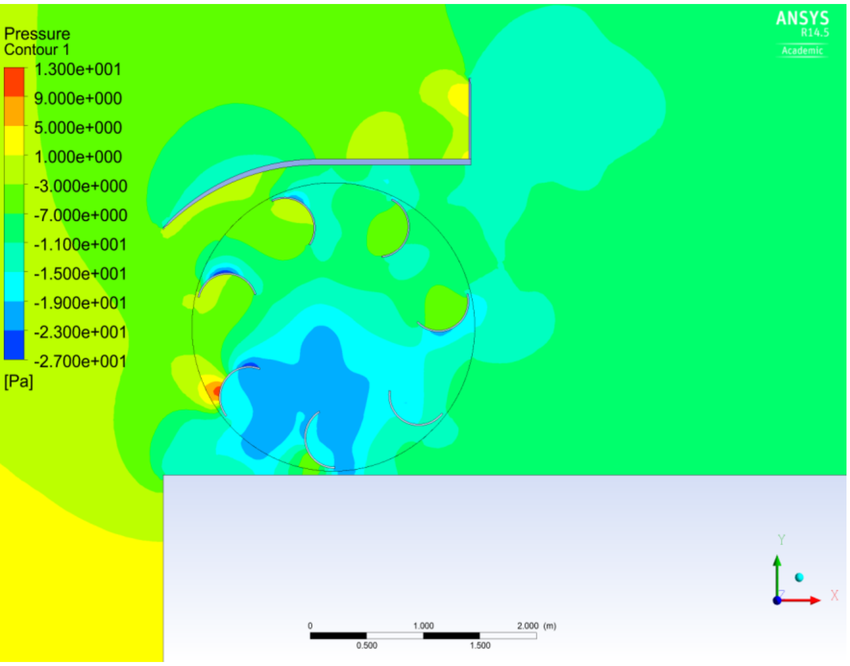

Figure 4.36: Pressure plot of case where $\theta_{cut} = 30°$

4.2.3. NUMBER OF BLADES

An increase in the number of blades would increase the net surface area available for power generation, but it would also lead to more pressure build up within the turbine casing. In the paradigm of a turbine inside a casing/shroud, pressure build up is of extreme importance, as it can reduce the flow entering the turbine. Thus it is worth studying the correct number of blades that finds the balance between these two effects.

In this study the output performance of the turbine C_p is monitored. It is worth remarking that in the situation where two setups give the same output performance, the setup having less number of blades is preferred. This is because of the savings in cost of manufacture and transport. Four different set-ups were used for the purpose of analysis. For this analysis, the tip speed ratio, $\lambda = 0.5$ and free stream velocity of wind at the height of the turbine is $v_{\infty} = 3.89\frac{m}{s}$.

Table 4.6 shows the number of blades N_{blades} of each set up.

Setup	$\boldsymbol{N_{blades}}$
1	5
2	6
3	7
4	8

Table 4.6: Number of blades N_{blades} for each configuration

Figures 4.37 through 4.40 show the instantaneous velocity streamlines for each set up. Furthermore, Figure 4.41 presents the variation of turbine output performance C_p with the number of blades N_{blades} and finds the optimal number of blades $N_{blades_{opt}} = 7$ for this particular turbine.

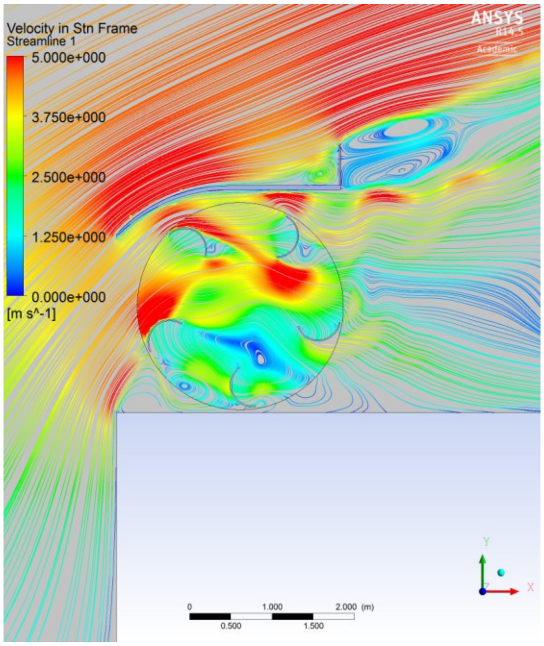

Figure 4.37: Instantaneous velocity streamlines for $N_{blades} = 5$

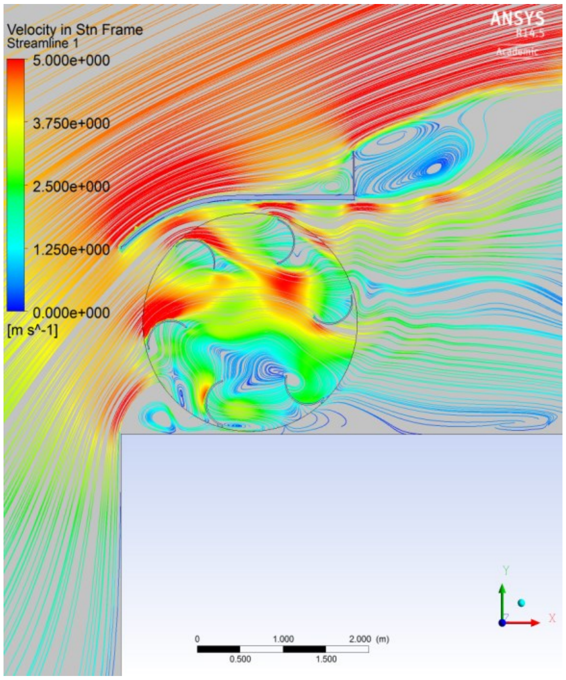

Figure 4.38: Instantaneous velocity streamlines for $N_{blades} = 6$

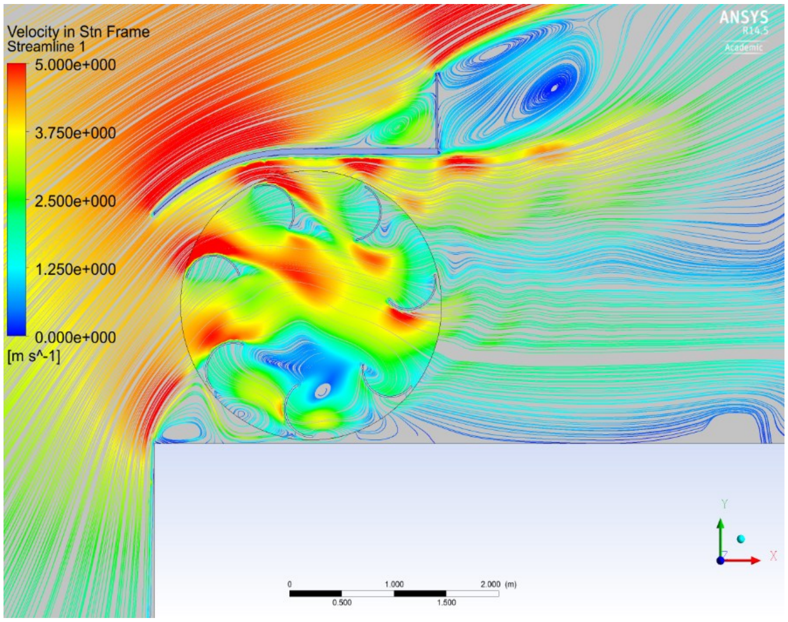

Figure 4.39: Instantaneous velocity streamlines for $N_{blades} = 7$

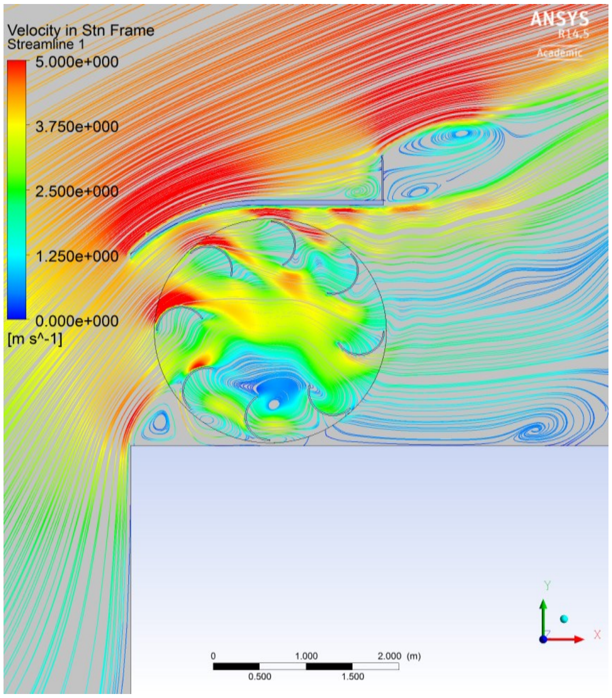

Figure 4.40: Instantaneous velocity streamlines for $N_{blades} = 8$

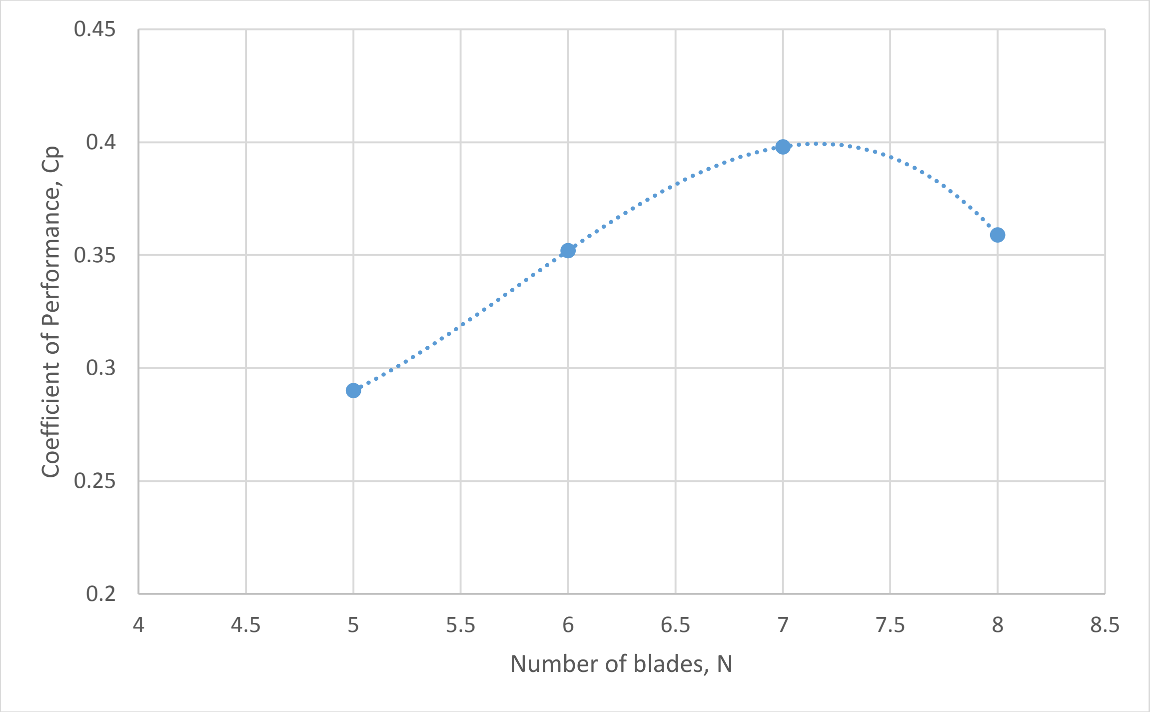

Figure 4.41: Plot showing variation of C_p with change in number of blades N_{blades}

4.2.4. POSITION OF TURBINE

The turbine location inside the shroud directly impacts the output performance of the turbine. It is ideal to locate the turbine such that the blades are able to capture the accelerated flow over the roof at the correct angle. In order to study this, the turbine is displaced horizontally, while monitoring the output performance C_p of the turbine.

Figure 4.42 shows the schematic of the turbine in the shroud with relevant parameters labelled. Here d refers to the horizontal displacement of the turbine rotor from the edge of the building. The tip radius of the turbine rotor R is $1.25m$.

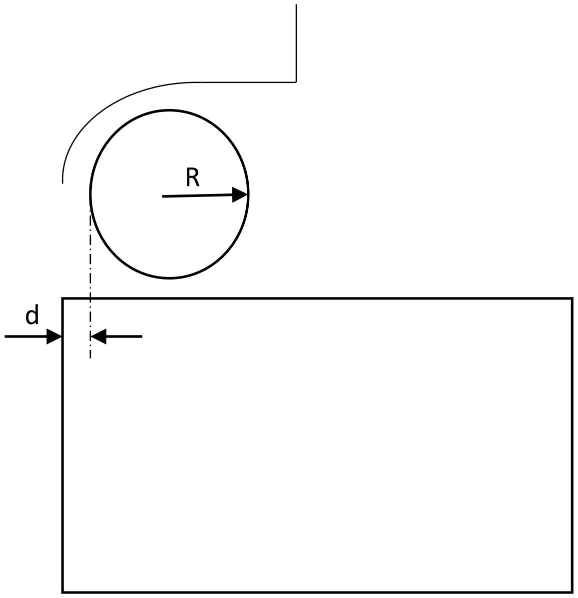

Figure 4.42: Schematic showing horizontal displacement of turbine rotor d and the radius of the turbine rotor R

Four different set-ups were used for the purpose of analysis. For this analysis, the tip speed ratio, $\lambda = 0.5$ and free stream velocity of wind at the height of the turbine is $v_\infty = 3.89\,\frac{m}{s}$.

Table 4.7 shows the horizontal displacement d along with the ratio $\frac{d}{R}$ of each set up.

Configuration	Horizontal displacement d(m)	$\frac{d}{R}$
1	0	0
2	0.125	0.1

3	0.25	0.2
4	0.375	0.3

Table 4.7: Horizontal displacement d of the rotor and ratio $\frac{d}{R}$ of each setup

Figures 4.43 through 4.46 show the instantaneous velocity streamlines for each set up. Furthermore, Figure 4.47 presents the variation of turbine output performance C_p with the ratio $\frac{d}{R}$ and finds the optimal ratio $\frac{d}{R_{opt}} = 0.2$ for this particular turbine.

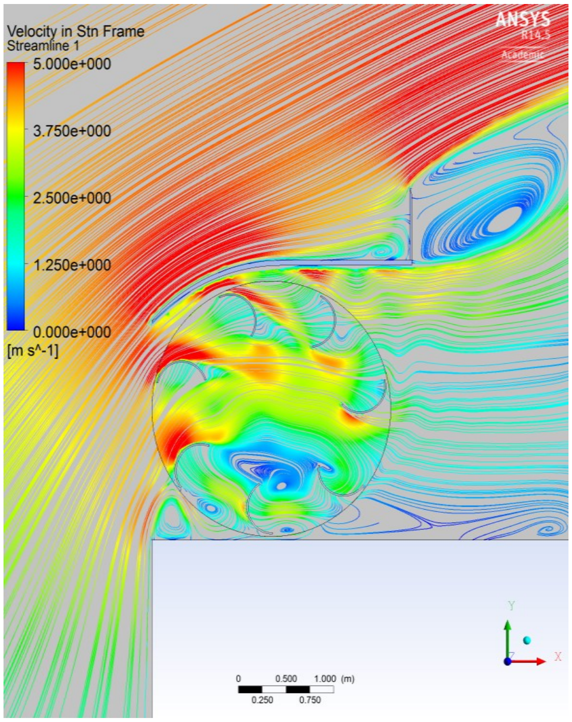

Figure 4.43: Instantaneous velocity streamlines for $\frac{d}{R} = 0$

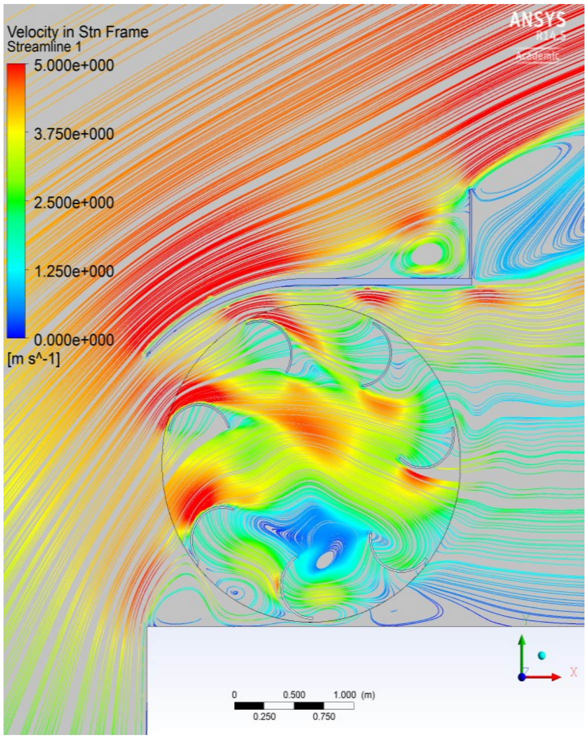

Figure 4.44: Instantaneous velocity streamlines for $\frac{d}{R} = 0.1$

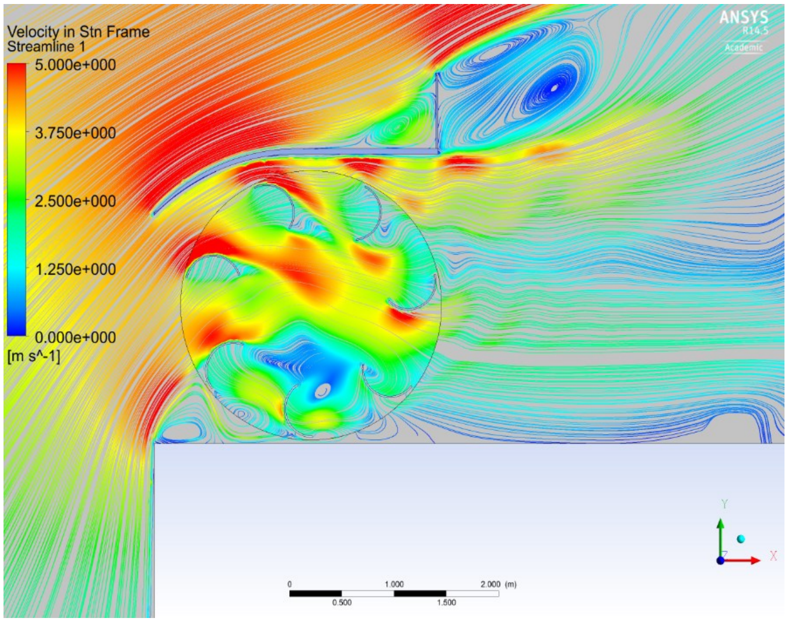

Figure 4.45: Instantaneous velocity streamlines for $\frac{d}{R} = 0.2$

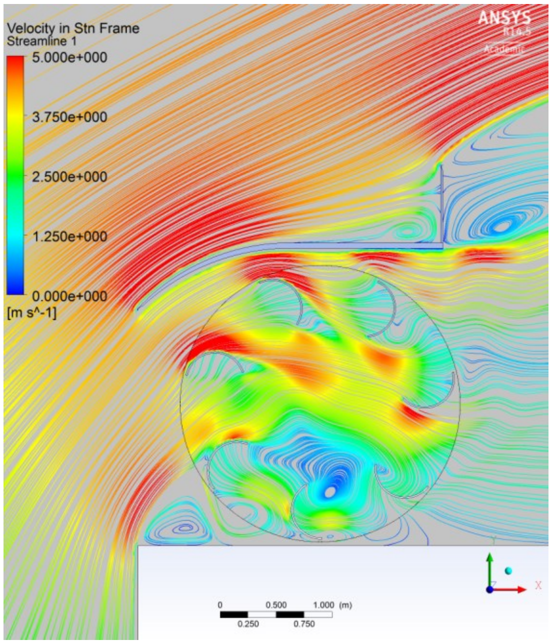

Figure 4.46: Instantaneous velocity streamlines for $\frac{d}{R} = 0.3$

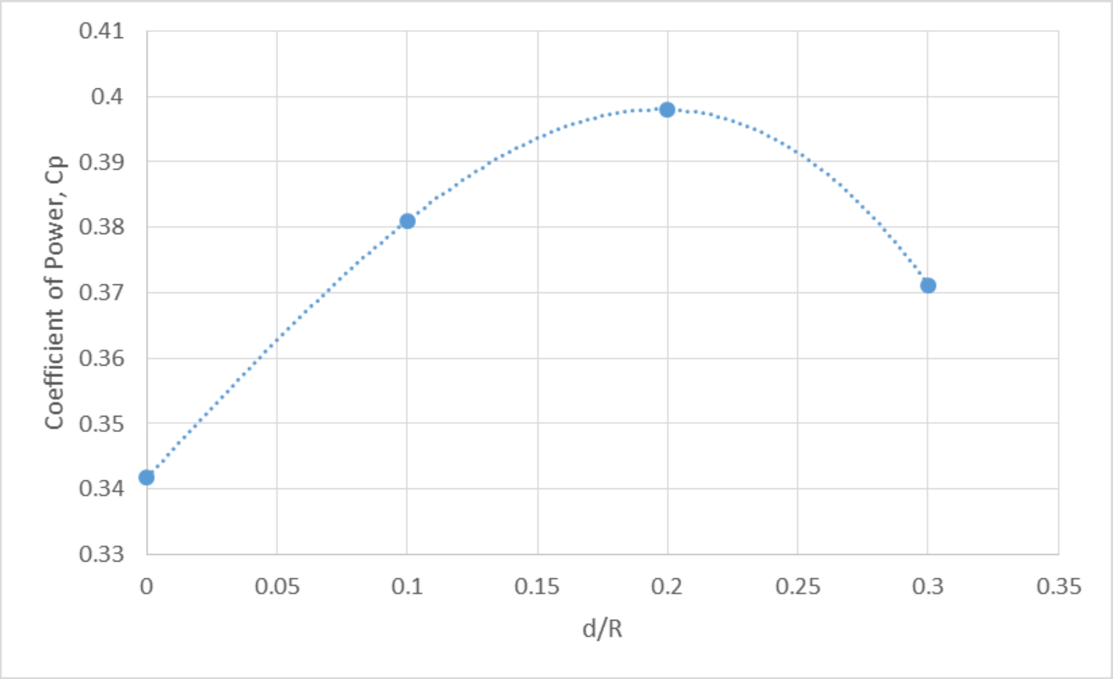

Figure 4.47: Plot showing the variation of C_p with change in $\frac{d}{R}$

4.3. FINAL DESIGN

In this section, the final design is presented. This design is arrived at, after additively including all the design changes from the non-dimensional parametric studies discussed in the previous chapter. It is worth mentioning here that although it was found that the angled shape of the diffuser provides a slightly higher power output, the straight diffuser was chosen for ease of manufacture. However this is most definitely an area for future research.

Table 4.8. shows the non-dimensional values of this design.

Non-dimensional parameter	**Value**
$\frac{h}{H}$	0.273
$\frac{y}{Y}$	0
$\frac{L}{H}$	1
θ_{cut}	$30\,°$
N_{blades}	7
$\frac{d}{R}$	0.2

Table 4.8: Non dimensional design parameters of final design

Figure 5.1 shows the instantaneous velocity streamlines for this set up. Here the tip speed ratio, $\lambda = 0.5$ and free stream velocity of wind at the height of the turbine is $3.89\frac{m}{s}$.

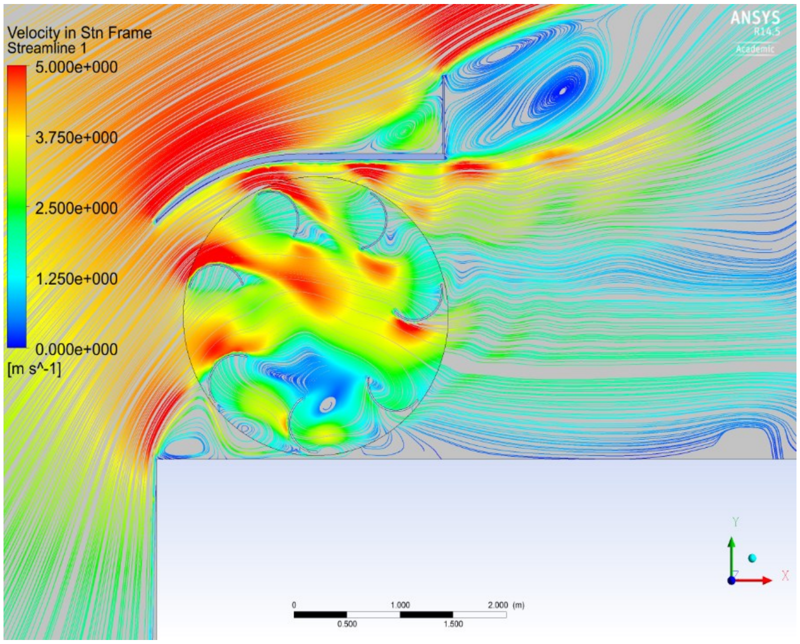

Figure 4.48: Instantaneous velocity streamlines for final design

It is seen that the coefficient of power of this design is $C_{p_{final}} = 0.394$, which is considerably higher than that of the initial design (before the changes). $C_{p_{initial}} = 0.135$.

5.2. OPTIMAL TIP SPEED RATIO

Since the tip speed ratio λ is a variable that can be controlled for different velocities, a study is conducted to find the optimum tip speed ratio for the operation of this turbine at the free stream velocity of $3.89\frac{m}{s}$.

Five different set-ups were used for the purpose of analysis. For this analysis, the free stream velocity of wind at the height of the turbine is $v_\infty = 3.89\frac{m}{s}$.

Table 5.2 shows the tip speed ratio λ of each set up.

Setup	**Tip Speed Ratio, λ**
1	0.33
2	0.38
3	0.45
4	0.5
5	0.6

Table 4.9: Tip Speed Ratio values for each configuration in the study

Figure 5.2 presents the variation of turbine output performance C_p with the tip speed ratio λ for this particular turbine at the free stream velocity $v_\infty = 3.89\frac{m}{s}$.

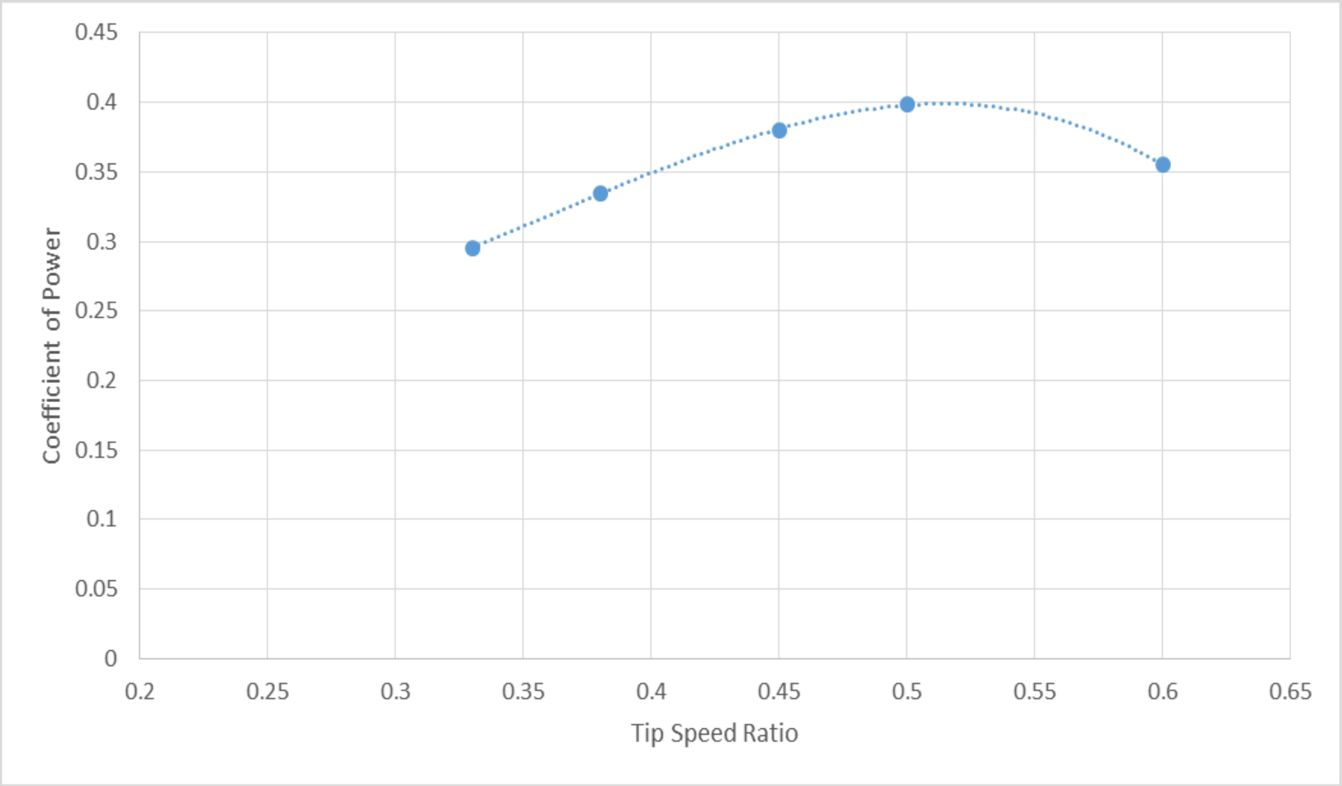

Figure 4.49: Plot showing variation of C_p with change in tip speed ratio λ

Thus we see that, with $\lambda = 0.5$, we obtain $C_p = 0.4$ which is almost three times the power output of the initial turbine design. This validates the design changes that have been recommended through the course of this thesis and shows the efficiency of this turbine design.

CHAPTER 5 : CONCLUSION

In this thesis, a rooftop turbine (VAWT oriented horizontally) is analyzed. An appropriate model is chosen with the meshing strategy and turbulence model being clearly defined. A grid convergence study is conducted to ensure independence of solution from the grid resolution, as well as to ensure that the solutions obtained are within the asymptotic range of convergence. Next, 3D simulations of a rooftop-mounted turbine are conducted. The emphasis is placed on the turbine casing, and the blades of the turbine, with the objective to improve power output (and hence, efficiency) of the turbine. Non dimensional parametric studies are conducted on each of the design parameters of the components of the turbine, with the coefficient of power C_p being the key variable. The results of these studies allow us to present a final design that shows considerable improvement (almost 300%) over the initial design. It is worth mentioning that no such design has been studied in the past. The final power coefficient $C_p = 0.394$ that is obtained, is better than even horizontal axis wind turbines (HAWT) of the same size, and in the same range as much larger HAWTs.

5.1. SCOPE OF FUTURE STUDY

The following areas are recommended for future research through numerical analysis :

1. A multi-objective optimization study to find the correlation between each of the non-dimensional parameters that have been studied in this thesis. For the purpose of this thesis, only one parameter was varied in each study, while the others remained constant. However, it is interesting to study how the results found would vary, if all the parameters were allowed to change simultaneously.

2. A vortex forms on the side of the wall, which is also seen to contribute to the low pressure region around the turbine. This enhances the suction effect, increasing the mass flux of air into the turbine. A numerical analysis to study this effect of the side vortex could be extremely beneficial.
3. While the walls of the diffuser have been kept straight for this thesis, it has been shown before that curved walls are capable of producing more accelerating effect. This impact of the curved walls is a worthwhile focal point of research.
4. It is also interesting to study arrays of such rooftop turbines, and to see the interaction of flow due to the presence of multiple turbines on the same roof.

REFERENCES

[1] E. Vine, "Breaking down the silos: the integration of energy efficiency, renewable energy, demand respnose and climate change," Energy Efficiency, pp. 49-63, 2008.

[2] C. Q. Choi, "Gulf oil spill paves way for alternative energy push," 10 June 2010. [Online]. Available: http://www.livescience.com/6572-gulf-oil-spill-paves-alternative-energy-push.html.

[3] W. Zhou, C. Lou, Z. Li, L. Lu and H. Yang, "Current status of research on optimum sizing of stand-alone hybrid solar-wind power generation systems," Applied Energy, pp. 380-389, 2010.

[4] A. Strupczewski, "Accident risks in nuclear-power plants," Applied Energy, pp. 79-86, 2003.

[5] A. Evans, V. Strezov and T. J. Evans, "Assessment of sustainability indicators for renewable energy technologies," Renewable and Sustainable Energy Reviews, pp. 1082-1088, 2009.

[6] R. Langton, I. M. Davies and B. E. Scott, "Seabird conservation and tidal stream and wave power generation: Information needs for predicting and managing potential impacts," Marine Policy, pp. 623-630, 2011.

[7] G. M. Shafiullah, A. M. T. Oo, A. B. M. S. Ali and P. Wolfs, "Potential challenges of integrating large-scale wind energy into the power grid - A review," Renewable and Sustainable Energy Reviews, pp. 306-321, 2013.

[8] H. Long, X. Li, H. Wang and J. Jia, "Biomass resources and their bioenergy potential estimation: A review," Renewable and Sustainable Energy Reviews, pp. 344-352, 2013.

[9] E. Toklu, "Overview of potential and utilization of renewable energy sources in Turkey," Renewable Energy , pp. 456-463, 2013.

[10] T. E. Boukelia and M.-S. Mecibah, "Parabolic trough solar thermal power plant: Potential, and projects development in Algeria," Renewable and Sustainable Energy Reviews, pp. 288-297, 2013.

[11] Y. d. Boer, "The Energy Report 2013 : 100% Renewable by 2050," 2013. [Online]. Available: http://wwf.panda.org/what_we_do/footprint/climate_carbon_energy/energy_solutions22/renewable_energy/sustainable_energy_report/.

[12] R. Bãnos, F. Manzano-Agugliaro, F. G. Montoya, C. Gil, A. Alcayde and J. Gómez, "Optimization methods applied to renewable and sustainable energy: A review," Renewable and Sustainable Energy Reviews, pp. 1753-1766, 2011.

[13] The Renewable Energy Policy Network for the 21st Century (REN21), "Renewables Global Status Report," 2010.

[14] S. N. Zadeh, Mesh Requirement Investigation for 2D and 3D Aerodynamic Simulation of Vertical Axis Wind Turbines : MASc Thesis, Montréal: Concordia University, 2013.

[15] G. W. E. Council and G. International, "Global Wind Energy Outlook," 2010.

[16] Conserve Energy Future, "Disadvantages of Renewable Sources of Energy," [Online]. Available: http://www.conserve-energy-future.com. [Accessed 19 May 2015].

[17] S. Eriksson, H. Bernhoff and M. Leijon, "Evaluation of different turbine concepts for wind power," Renewable and Sustainable Energy Reviews, vol. 12, no. 5, pp. 1419-1434, 2006.

[18] I. Paraschivoiu, Wind Turbine Design with Emphasis on Darrieus Concept, Montreal: Polytechnic International Press, Canada, 2002.

[19] S. Mathew, Wind Energy Fundamentals, Resource Analysis and Economics, Netherlands: Springer, 2006.

[20] M. C. Claessens, "The Design and Testing of Airfoils for Application in Small Vertical Axis Wind Turbines," Delft University of Technology, Amsterdam, 2006.

[21] L. Ledo, P. B. Kosasih and P. Cooper, "Roof mouting site analysis for micro-wind turbines," Renewable Energy, vol. 36, no. 5, pp. 1379-1391, 2011.

[22] L. Soder, L. Hofmann, A. Orths, H. Holttinen, Y.-h. Wan and A. Tuohy, "Experience from wind integration in some high penetration areas," IEEE Transactions on Energy Conversion, vol. 1, no. 22, pp. 4-12, 2007.

[23] B. Sanderse, S. P. v. d. Pijl and B. Koren, "Review of computational fluid dynamics for wind turbine wake aerodynamics," Wind Energy, no. 14, pp. 799-819, 2011.

[24] C. Song, Y. Zheng, Z. Zhao, Y. Zhang, C. Li and H. Jiang, "Investigation of meshing strategies and turbulence modesl of computational fluid dynamics simulations of vertical axis wind turbines," Journal of Renewable and Sustainable Energy, no. 7, 2015.

[25] E. Sagol, M. Reggio and A. Ilinca, "Assessment of Two-Equation Turbulence Models and Validation of the Performance Characteristics of an Experiemental Wind Turbine by CFD," ISRN Mechanical Engineering, 2012.

[26] E. S. Holdredge and B. H. Reed, "Pressure Distribution on Buildings," Texas Engineering Experimental Station, College Station, 1957.

[27] B. H. Evans, "Natural Air Flow around Buildings," Texas Engineering Experimental Station, College Station, 1957.

[28] C. C. S. Song and J. He, "Computation of Wind Flow around a Tall Building and the Large-Scale Vortex Structure," Journal of Wind Engineering and Industrial Aerodynamics, no. 46; 47, pp. 219-228, 1993.

[29] A. A. Razak, A. Hagishima, N. Ikegaya and J. Tanimoto, "Analysis of airflow over buildng arrays for assessment of urban wind environment," Building and Environment, no. 59, pp. 56-65, 2013.

[30] I. Abohela, N. Hamza and S. Dudek, "Effect of roof shape, wind direction, building height and urban configuration on the energy yield and positioning of roof mounted wind turbines," Renewable Energy, no. 50, pp. 1106-1118, 2013.

[31] I. Abohela, N. Hamza and S. Dudek, "Roof Mounted Wind Turbines: A methodology for assessing potential roof mounting locations," in 29th Conference, Sustainable Architecture for a Renewable Future, Munich, 2013.

[32] Y. Ohya, T. Karasudani and X. Zhang, "A Shrouded Wind Turbine generating high output power with Wind Lens technology," Energies, vol. 3, pp. 634-640, 2010.

[33] R. E. Wilson and P. B. S. Lissaman, "Applied Aerodynamics of Wind Power Machines," Oregon State University, Portland, 1974.

[34] C. S. Ferreira, H. A. Madsen, M. Barone, B. Roscher, P. Deglaire and I. Arduin, "Comparison of aerodynamic models for vertical axis wind turbines," in The Science of Making Torque from Wind, Copenhagen, 2014.

[35] N. N. Sorensen, J. A. Michelsen and S. Schreck, "Navier-Stokes predictions of the NREL phase VI rotor in the NASA Ames 80ftx20ft wind tunnel," Wind Energy, vol. 5, no. 2-3, pp. 151-169, 2002.

[36] T. H. Shih, W. W. Liou, A. Shabbir, Z. Yang and J. Zhu, "A New k-epsilon eddy viscosity model for high Reynolds number turbulent flows-Model Development and Validation," Computers Fluids, vol. 24, no. 3, pp. 227-38, 1995.

[37] A. Digraskar, "Simulations of Flow Over Wind Turbines," University of Massachusetts, MSc Thesis, Amherst, 2010.

[38] M. J. Aftosmis, D. Gaitonde and T. S. Tavares, "On the accuracy, stability and montonicity of various reconstruction algorithms for unstructured meshes," in 32nd AIAA Aerospace Sciences Meeting and Exhibit, Reno, 1994.

[39] G. Bono and A. M. Awruch, "Numerical Study between Structured and Unstructured Meshes for Euler and Navier-Stokes Equations," Mecánica Computacional , vol. 26, pp. 3134-3146, 2007.

[40] ANSYS Inc. , "ANSYS FLUENT 12.0 User's Guide," 2009.

[41] P. J. Roache, Verifcation and Validation in Computational Science and Engineering, Hermosa Publications, 1998.

[42] K. Abe, H. Kihara, A. Sakurai, M. Nishida, Y. Ohya, E. Wada and K. Sato, "An experimental study of tip-vortex structures behind a small wind turbine with a flanged diffuser," Wind and Structures, vol. 9, no. 5, pp. 413-417, 2006.

[43] K. Abe, M. Nishida, A. Sakurai, Y. Ohya, H. Kihara, E. Wada and K. Sato, "Experimental and numerical investigations of flow fields behind a small-type wind turbine with flanged diffuser," Journal of Wind Engineering and Industrial Aerodynamics, vol. 93, pp. 951-970, 2005.

[44] O. Igra, "Research and development for shrouded wind turbines," Energy Conversion and Management, vol. 21, pp. 13-48, 1981.

[45] B. L. Gilbert and K. M. Foreman, "Experiments with a diffuser-augmented model wind turbine," Transactions of the ASME, Journal of Energy Resources Technology, vol. 105, pp. 46-53, 1983.

[46] I. C. Mandis, D. N. Robescu and M. Bãrglãzan, "Capitalization of wind potential using a modified Banki wind turbine," UPB Scientifical Bulletin, Series D: Mechanical Engineering, vol. 70, no. 4, pp. 115-124, 2008.

[47] A. Dragomirescu, "Performance assessment of a small wind turbine with crossflow runner by numerical simulations," Renewable Energy, vol. 36, pp. 957-965, 2011.